Received: 3 June 2021 | Revised: 26 July 2021 | Accepted: 20 September 2021

DOI: 10.1002/dneu.22852

RESEARCH ARTICLE

WILEY

Insights into the genetic regulatory network underlying neurogenesis in the parthenogenetic marbled crayfish *Procambarus virginalis*

Georg Brenneis[1,2] | **Martin Schwentner**[3,4] | **Gonzalo Giribet**[4] | **Barbara S. Beltz**[1]

[1] Neuroscience Program, Wellesley College, Wellesley, Massachusetts, USA

[2] Zoologisches Institut und Museum, Universität Greifswald, Greifswald, Germany

[3] Naturhistorisches Museum Wien, Vienna, Austria

[4] Department of Organismic and Evolutionary Biology, Museum of Comparative Zoology, Harvard University, Cambridge, Massachusetts, USA

Correspondence
Georg Brenneis and Barbara S. Beltz, Neuroscience Program, Wellesley College, 106 Central Street, Wellesley, MA 02481, USA.
Email: georg.brenneis@posteo.de and bbeltz@wellesley.edu

Funding information
Deutsche Forschungsgemeinschaft, Grant/Award Numbers: BR5039/1-1, BR5039/3-1; Museum of Comparative Zoology (Harvard University); National Science Foundation, Grant/Award Number: NSF-IOS-1656103

Abstract

Nervous system development has been intensely studied in insects (especially *Drosophila melanogaster*), providing detailed insights into the genetic regulatory network governing the formation and maintenance of the neural stem cells (neuroblasts) and the differentiation of their progeny. Despite notable advances over the last two decades, neurogenesis in other arthropod groups remains by comparison less well understood, hampering finer resolution of evolutionary cell type transformations and changes in the genetic regulatory network in some branches of the arthropod tree of life. Although the neurogenic cellular machinery in malacostracan crustaceans is well described morphologically, its genetic molecular characterization is pending. To address this, we established an in situ hybridization protocol for the crayfish *Procambarus virginalis* and studied embryonic expression patterns of a suite of key genes, encompassing three *SoxB* group transcription factors, two *achaete–scute* homologs, a *Snail* family member, the differentiation determinants *Prospero* and *Brain tumor*, and the neuron marker *Elav*. We document cell type expression patterns with notable similarities to insects and branchiopod crustaceans, lending further support to the homology of hexapod–crustacean neuroblasts and their cell lineages. Remarkably, in the crayfish head region, cell emigration from the neuroectoderm coupled with gene expression data points to a neuroblast-independent initial phase of brain neurogenesis. Further, *SoxB* group expression patterns suggest an involvement of *Dichaete* in segmentation, in concordance with insects. Our target gene set is a promising starting point for further embryonic studies, as well as for the molecular genetic characterization of subregions and cell types in the neurogenic systems in the adult crayfish brain.

KEYWORDS
achaete–scute homolog, brain tumor, development, Elav, nervous system, neuroblast, Prospero, Snail, SoxB

1 | INTRODUCTION

Developmental studies on the central nervous system (CNS) of *Drosophila melanogaster* and other representatives of the Hexapoda (insects and kin) have provided considerable insights into the genetic regulatory network (GRN) of neurogenesis and into mechanisms of stem cell self-renewal and maintenance as well as neural differentiation (Crews, 2019; Homen & Knoblich, 2012; Kang & Reichert, 2015). Comparative works on other major arthropod groups (i.e., Chelicerata, Myriapoda, crustaceans) have revealed a notable degree of GRN conservation and shed light on the evolution of the different cell types involved in neurogenesis (Stollewerk, 2016). However, limited data for some groups still impact the resolution level of evolutionary changes and hamper the underpinning of cell type homology with equivalent data classes. Among the understudied groups regarding the neurogenic GRN are crustaceans, the closest relatives of Hexapoda, with which they form the clade Tetraconata or Pancrustacea (e.g., Schwentner et al., 2017, 2018).

In hexapods, embryonic neurogenesis is mainly driven by stem cell-like neural progenitors, the neuroblasts (NBs). Each NB emigrates from the single-layered neuroectoderm (NE) into a subapical position and starts to divide repeatedly in asymmetrical fashion, giving rise to an invariant lineage of ganglion mother cells (GMCs) (Figure 1e). GMCs in turn divide typically only once to generate two postmitotic neural precursors (terminology sensu Hartenstein & Stollewerk, 2015), which differentiate into neurons and/or glial cells. In several crustacean taxa (including Malacostraca, Branchiopoda, and Copepoda), NBs and GMCs with similar division modes drive neurogenesis (Dohle, 1976; Hein & Scholtz, 2018; McMurrich, 1895; Scholtz, 1990, 1992; Ungerer & Scholtz, 2008; Ungerer, Eriksson, et al., 2011). However, these crustacean NBs remain in the apical NE during their divisions (Figure 1e) and their homology to hexapod NBs has long been contested (see Ungerer & Scholtz, 2008). By now, NB homology is more generally accepted, owing to similarities between entire NB cell lineages (Ungerer & Scholtz, 2008), sets of stereotypical pioneer neurons generated (e.g., Thomas et al., 1984; Whitington et al., 1993, 1996), and the first molecular investigations in crustaceans (Duman-Scheel & Patel, 1999; Ungerer, Eriksson, et al., 2011; Ungerer et al., 2012; Wheeler & Skeath, 2005). According to recent insights into pancrustacean phylogeny (Schwentner et al., 2017, 2018), NB-driven neurogenesis can thus be traced to the last common ancestor of Altocrustacea (a clade that includes Malacostraca, Branchiopoda, Hexapoda as well as other crustacean lineages), and the subapical immigration of NBs represents a derived state in hexapods (Brenneis et al., 2013; Hein & Scholtz, 2018).

The Malacostraca comprises several traditional models for developmental and neurobiological research, such as crayfish (review: Harzsch et al., 2015). Although the cellular machinery driving malacostracan neurogenesis is better characterized than in any other crustacean group (see, e.g., Ungerer & Scholtz, 2008), the GRN underlying neurogenic processes has not been studied. This hampers comparison with branchiopods (Ungerer, Eriksson, et al., 2011; Ungerer et al., 2012; Wheeler & Skeath, 2005) and elucidation of common genetic regulatory principles of the ancestral mode of pancrustacean CNS development. Remarkably, some malacostracans also display adult neurogenesis, the persistent generation of neurons in specialized proliferation centers in the brain of mature animals (reviews: Sandeman et al., 2011; Wittfoth & Harzsch, 2018), which is not reported for any other crustacean group. These adult neurogenic systems are best known in the Decapoda, especially in crayfish and spiny lobsters (Chaves da Silva et al., 2012; Schmidt, 2001; Sullivan & Beltz, 2005; Sullivan, Benton, et al., 2007; Sullivan, Sandeman, et al., 2007), but the neural progenitor types at their base appear to differ between taxa (Benton et al., 2011, 2014; Brenneis & Beltz, 2020; Schmidt, 2007; Schmidt & Derby, 2011; Wittfoth & Harzsch, 2018) and a molecular genetic characterization is pending.

In the last two decades, the marbled crayfish *Procambarus virginalis* Lyko, 2017, previously *P. fallax* f. *virginalis* (see Lyko, 2017; Martin et al., 2010), has emerged as a new laboratory model for crayfish studies. It is the only known parthenogenetic decapod crustacean (Scholtz et al., 2003); all individuals are female, show high fertility under laboratory conditions, and produce genetically identical offspring (Martin et al., 2007; Seitz et al., 2005; Vogt et al., 2015). *Procambarus virginalis* is a triploid organism (Martin et al., 2016; Vogt et al., 2015) and a draft genome has recently become available (Gutekunst et al., 2018). Despite triploidy and a parthenogenetic reproduction mode, no deviations from the development previously documented for crayfish are known (Alwes & Scholtz, 2006; Reichenbach, 1886; Sandeman, & Sandeman, 1991; Seitz et al., 2005; Zehnder, 1934): The early germ disc forms by condensation of the blastoderm. It comprises the primordia of the optic lobes and the three naupliar segments, posteriorly bordered by the incipient caudal papilla (Figures 1a and 2a). After germ disc condensation, the anlagen of the three naupliar limb pairs (antennae 1 and 2, mandibles) start to bulge out (Figure 1b) and in the caudal papilla, a ring of about 40 stem cell-like dividing ectoteloblasts (ETs) begins to differentiate (Alwes & Scholtz, 2006; Scholtz, 1992, 1993). These ETs are the source (of most) of the future ectodermal cell material in the postnaupliar region. Each ET divides in an asymmetrical fashion to anteriorly "bud off" a daughter cell (cell row "abcd"; Figure 1d) that

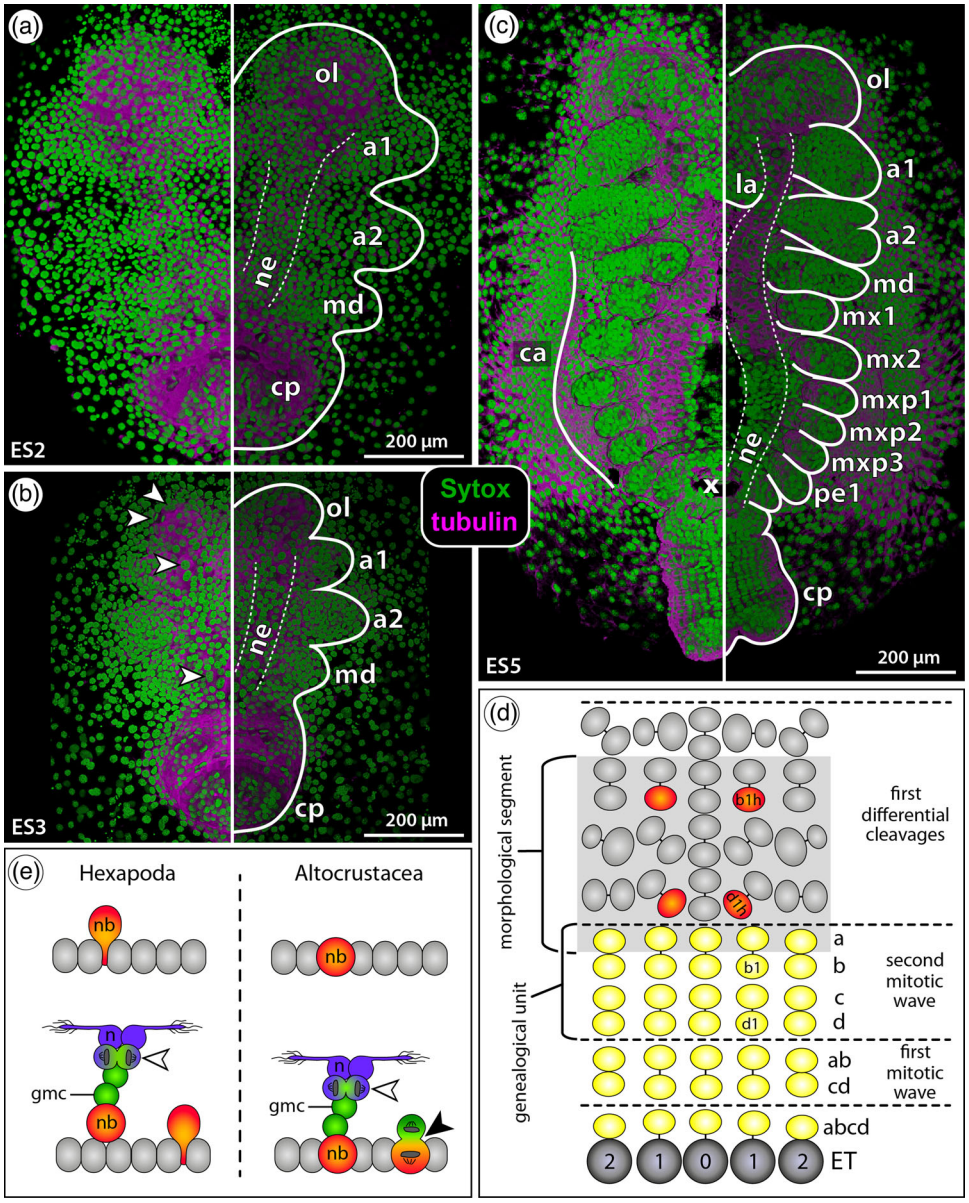

FIGURE 1 Key characteristics of the embryonic development of *P. virginalis*. (a–c) Selected embryonic stages in ventral view, tubulin immunolabeling (magenta) with Sytox nuclear counterstain (green); Imaris volumes (blend) of CLSM scans. (a) Advanced stage 2. The germ disc comprises the anlagen of the optic lobe and the three naupliar segments, followed by the caudal papilla. The naupliar NE is V-shaped and stretches from the optic lobe to the posterior border of the mandibular segment. (b) Stage 3. Owing to compaction of cells, the embryo diminishes in overall size. The naupliar limb buds and caudal papilla start to bulge out. In the apical layer of the optic lobe and naupliar NE, the first cells with enlarged nuclei (arrowheads) become discernible. (c) Stage 5. In the postnaupliar region, the segments up to the first pereiopods bear distinct limb buds. In the caudal papilla, further segmental anlagen are being added. (d) Cell division patterns during postnaupliar segment formation; only midline and flanking neuroectodermal cell columns 1 and 2 shown, posterior to the bottom. The ETs (dark gray) divide asymmetrically to give rise to cell row "abcd" (yellow). Two waves of longitudinally oriented symmetrical divisions result in the four cell rows "a" to "d" (yellow). The first differential divisions show deviating but stereotypical orientations (light gray) and the first NBs b1h and d1h are being formed (orange). The borders of genealogical units and the later morphological segments are not aligned. (e) Early neurogenesis in the ventral NE of Hexapoda (left), compared to the ground pattern of Altocrustacea (right). Hexapod NBs (orange) are specified in the apical NE and emigrate to a subapical position before starting to generate GMCs (green) via asymmetrical divisions. GMCs in turn divide just once to produce postmitotic neurons and/or glia (blue). In the remaining altocrustacean taxa, NBs remain within the apical neuroectodermal cell layer while budding off the GMCs. Abbreviations: a1 and a2, antenna1 and 2 segments; ca, carapace; cp, caudal papilla; ET, ectoteloblast; gmc, ganglion mother cell; la, labrum; md, mandibular segment; mx1 and mx2, maxilla 1 and 2 segments; mxp1–3, maxilliped 1–3 segments; n, neuron; nb, neuroblast; ne, neuroectoderm; ol, optic lobe; pe1, pereiopod 1 segment

TABLE 1 Target gene/gene families and their location of expression and functions during neurogenesis in Hexapoda and—if known—branchiopod crustaceans

Gene/gene family	Location of expression in Hexapoda and Branchiopoda	Function(s) in Hexapoda and Branchiopoda	Sources
SoxB group	Broad expression across major parts of the NE ("NE marker")	Proneural; NE patterning; NB formation	Arefin et al., 2019; Buescher et al., 2002; Crémazy et al., 2000; Janssen et al., 2018; Overton et al., 2002; Zhao et al., 2007; Zhao & Skeath, 2002
Achaete–scute complex			
ASH	Proneural cell clusters in NE and/or nascent NBs	Proneural	Cabrera et al., 1987; Jiménez & Campos-Ortega, 1990; Negre & Simpson, 2009; Skeath & Carroll, 1992; Skeath & Thor, 2003; Ungerer, Eriksson, et al., 2011; Wheeler et al., 2003; Wheeler & Skeath, 2005
Ase(-like)	Persistent in differentiated NBs ("NB marker")	NB self-renewal	Biffar & Stollewerk, 2014; Brand et al., 1993; Jarman et al., 1993; Southall & Brand, 2009; Ungerer, Eriksson, et al., 2011; Ungerer et al., 2012; Wheeler et al., 2003; Wheeler & Skeath, 2005
Snail family	NE, especially in forming and differentiated NBs	Proneural; maintenance of NB self-renewal; asymmetrical NB division	Arefin et al., 2019; Ashraf et al., 1999; Ashraf & Ip, 2001; Cai et al., 2001; Lai et al., 2012; Southall & Brand, 2009; Ungerer, Eriksson, et al., 2011
Pros	NBs and GMCs, *Pros* protein segregated into GMC during NB divisions	Suppression of self-renewal genes; activation of neural differentiation genes	Choksi et al., 2006; Doe et al., 1991; Knoblich et al., 1995; Li & Vaessin, 2000; Liu et al., 2020; Spana & Doe, 1995; Ungerer, Eriksson, et al., 2011; Vaessin et al., 1991
Brat	NBs, GMCs, and maturating neurons, *Brat* protein segregated into GMC during NB divisions	Suppression of self-renewal genes	Bello et al., 2006; Betschinger et al., 2006; Lee et al., 2006; Reichardt et al., 2018
Elav	Maturating and mature neurons ("neuron marker")	3′UTR extension of neuronal RNAs; different types of alternative splicing	Koushika et al., 1996; Lee et al., 2021; Robinow & White, 1988, 1991; Soller & White, 2003; Wei et al., 2020

divides in two longitudinally oriented mitotic waves to form a genealogical unit of four transverse cell rows named "a," "b," "c," and "d" (Figure 1d). During the following round of differential cleavages, the first deviations from the longitudinal orientation occur, which are nonetheless still invariant (Alwes & Scholtz, 2006; Scholtz, 1992) (Figure 1d). The genealogical units differentiate along an anteroposterior developmental gradient, and morphological segments bearing the primordia of the limb buds become recognizable (Figure 1c). Notably, the borders of the segments are not aligned with the genealogical units, extending instead between cell rows "a" and "b" (Figure 1d). The postnaupliar CNS derives from the progeny of the ventral midline ET (ET0) and its two adjacent ET1 and ET2, the first NBs being formed during the first differential cleavages (cells "b1h" and "d1h") as descendants of ET1 (Figure 1d) (Alwes & Scholtz, 2006; Scholtz, 1992).

To complement the morphological neurodevelopmental studies on *P. virginalis* (Biffis, 2017; Fabritius-Vilpoux et al., 2008; Sintoni et al., 2012; Vilpoux et al., 2006) and gain insights into the GRN of malacostracan neurogenesis, we investigated expression patterns of a suite of genes/gene families that are part of the conserved genetic toolkit of arthropod neurogenesis (Hartenstein & Stollewerk, 2015; Stollewerk, 2016). Target gene/gene family selection was guided by their putative location of expression and their putative function(s) during neurogenesis as deduced from comparative and functional studies, especially in hexapods (see Table 1 for details). The targets selected include:

1. the three closely related *SoxB* group transcription factors (TFs) *SoxNeuro*, *Dichaete*, and *Sox21b*, which contain a conserved DNA-binding domain, the high-mobility group (HMG) box (Crémazy et al., 2000; Sánchez-Soriano & Russell, 2000);
2. homologs of the *achaete–scute* complex, which encode TFs of the basic Helix–Loop–Helix (bHLH) family. In

hexapods, these genes are divided into two classes, the proneural *achaete–scute* homologs (*ASH*) and the *asense* (*ase*) gene (e.g., Negre & Simpson, 2009; Skeath & Thor, 2003);
3. members of the *Snail* TF family, which are characterized by a conserved carboxy-terminal region of five DNA-binding C2H2 zinc fingers (e.g., Kerner et al., 2009; Nieto, 2002);
4. the neural determinant *Prospero* (*Pros*), a TF with a divergent homeodomain (Chu-Lagraff et al., 1991);
5. the neural determinant *Brain tumor (Brat)*, a posttranscriptional regulator binding to mRNAs via its NHL (NCL-1, HT2A, LIN-41) domain (Loedige et al., 2015; Sonoda & Wharton, 2001);
6. the neuron marker *Embryonic lethal abnormal visual system* (*Elav*) (Campos et al., 1985), which has three conserved RNA-binding domains (Robinow et al., 1988).

Our findings on *P. virginalis* provide the first insights into the GRN underlying embryonic neurogenesis in malacostracan crustaceans and reveal characteristic expression patterns in the different cell types involved, which further underpin the homology of crustacean and hexapod NBs and GMCs. Beyond this, the suite of target genes/gene families is a promising starting point for the molecular genetic characterization of different subregions and cell types in the more complex adult neurogenic systems in the crayfish brain.

2 | MATERIAL AND METHODS

2.1 | Animal husbandry

A laboratory husbandry of *P. virginalis* was maintained in the Wellesley College Animal Care Facility at room temperature (RT) on a 12/12-h light/dark cycle. Animals were kept in artificial pond water (double-distilled water complemented with trace minerals and buffered with sodium bicarbonate) in aquaria containing gravel, stones, bricks, plastic tubes, and a few plastic plants as hiding spots. Egg-bearing females were separated into small extra tanks and the developmental stage of the embryos checked daily. The staging applied throughout the study follows Alwes and Scholtz (2006).

2.2 | Embryo fixation and dissection

Eggs were removed from the female's pleopods with forceps and transferred into 2-ml Eppendorf tubes containing 4% paraformaldehyde in phosphate-buffered saline (PFA/PBS; Boston BioProducts #BM-155). Tubes were immediately transferred into a water bath at 70˚C for 5 min, quickly placed on ice for 5 min, and then left at 4˚C for at least 20 min. After manual perforation of the partially detached egg membranes, embryos were placed on a shaker for 30 min to 2 h at RT in a mixture of PFA/PBS and heptane (50:50). Next, the aqueous layer was replaced by methanol and the tubes turned upside down several times, resulting in the removal of membranes still attached to the embryos. Following transfer into absolute methanol, embryos were gradually brought back into PFA/PBS for overnight fixation at RT on a horizontal shaker at low setting. On the next day, embryos were transferred into PBS, dehydrated in a graded methanol series (30%, 50%, 70%, 90%, and 100%), and stored at −20˚C until further use.

2.3 | Generation of developmental transcriptomes

Total RNA of *P. virginalis* embryos covering embryonic stages 1–10 (sensu Alwes & Scholtz, 2006) was extracted as outlined in Schwentner et al. (2017). Following spectrometric quality check, some samples were additionally subjected to phenol/chloroform extraction to improve RNA purity. Sequencing and de novo assembly of the *P. virginalis* developmental transcriptome was performed at Genewiz (South Plainsfield, NJ, USA). Additionally, a transcriptome of *Procambarus clarkii* (Girard, 1852), a close relative of *P. virginalis*, had been previously sequenced and de novo assembled (as described in Schwentner et al., 2017) from various embryonic stages and different adult tissues. Both transcriptomes and the draft genome of *P. virginalis* (v.04; Gutekunst et al., 2018) were used for identification of target gene sequences.

2.4 | Identification of target gene sequences and phylogenetic analyses

Using published sequences from other crustaceans (*Panulirus argus*, *Macrobrachium nipponense*, *Daphnia pulex*, *Triops longicaudatus*) and the hexapods *Drosophila melanogaster* and *Tribolium castaneum* as queries for BLAST searches, sequences of putative orthologs were extracted from the *P. virginalis* transcriptome and draft genome and the *P. clarkii* transcriptome in Geneious R10 (ver. 10.2.6; Biomatters, Ltd, Auckland, New Zealand, RRID: SCR_010519). Reciprocal searches of the best matching gene sequences were performed against the NCBI databases for further validation of gene identity. For the *SoxB*, *achaete–scute* complex, and *Snail* TF families with multiple closely related paralogs, phylogenetic analyses were performed to check orthology assignment. For this purpose, arthropod sequences of the different *Sox* family TFs (groups B–F), *achaete–scute* complex genes, and *Snail* superfamily (*Snail* and *Scratch*) members were downloaded from GenBank or for the amphipod *Parhyale hawaiensis* in

part extracted from a developmental transcriptome (kindly provided by A. Pavlopoulos). Amino acid sequences were aligned separately for each gene with MAFFT 7.471 (Katoh & Standley, 2013) using the L-INS-I option. Apart from the few conserved domains, the alignments featured large, ambiguously aligned sections. For this reason, phylogenetic analyses were focused on the conserved domains. Of *SoxB* group TFs, we selected the highly conserved HMG box domain (following Baudouin-Gonzalez et al., 2021; Janssen et al., 2018; Paese, Leite, et al., 2018; Zhong et al., 2011) (File S1). Of the *achaete–scute* complex genes, the conserved basic Helix 1 and Helix 2 regions of the bHLH domain as well as the C-terminal motif were included (following Ayyar et al., 2010; Negre & Simpson, 2009). In addition, seven conserved amino acids preceding the basic region as well as the last five conserved amino acid positions of the Loop (between Helices 1 and 2) and six amino acid positions following Helix 2 were included. Because the C-terminal motif is more variable, a second alignment was assembled and phylogenetically analyzed, excluding the C-terminal motif (Files S2 and S3). Of the *Snail* and *Scratch* TFs, only the zinc-finger domains were included in the analysis (following Hannibal et al., 2012; Wei et al., 2016), as they are the only conserved regions present in all superfamily members (File S4). Phylogenetic analysis for each gene was performed with MrBayes (ver. 3.2.7a; Ronquist et al., 2012), running with nruns = 4, nchains = 6 for 10^{*7} generations sampling every 1000th tree and discarding the first 25% of retained trees as burn-in. The best-fitting evolutionary model (LG + G for *SoxB* and *achaete–scute* complex; Dayhoff + I + G for Snail superfamily) was selected based on model selection implemented in MEGA-X (Kumar et al., 2018). Resulting trees were visualized and midpoint rooted with FigTree 1.4.3. All MrBayes analyses were carried out on the CIPRES Science Gateway v. 3.3 (Miller et al., 2010). The coding regions of the target genes have been deposited in GenBank (File S5).

2.5 | Reverse transcription PCR and synthesis of RNA probes

First-strand cDNA synthesis from *P. virginalis* total RNA was performed with ThermoScript™ reverse transcriptase (Invitrogen, #12236-014) according to the manufacturer's protocol. For PCR amplification of target sequences, Phusion High-Fidelity DNA polymerase and the 5× PCR buffers provided by the manufacturer were used (ThermoFisher Scientific; #F530L) together with gene-specific primers (File S6). Products were checked by gel electrophoresis and cleaned directly (Monarch PCR & DNA Cleanup Kit; New England Biolabs, #T1030S) or by gel purification (Monarch DNA Gel Extraction Kit, New England Biolabs, #T1020S). Purified products were cloned with a Zero Blunt TOPO PCR Cloning Kit with chemically competent TOP10 OneShot cells (ThermoFisher Scientific, Invitrogen, #K2875-20). After inoculation on LB/ampicillin agar plates at 37˚C, up to 10 clones were picked, streaked out on replica plates, and amplified with the M13 primers flanking the inserts on the vector. Products were checked for the expected fragment length and clones were selected to be grown in LB medium overnight at 37˚C with vigorous shaking. Plasmid purification was performed with a QIAprep Spin Miniprep Kit (QIAgen, #27106) according to the manufacturer's protocol. Purified plasmids were sent for sequencing at Genewiz to check insert orientation. Selected clones were linearized by PCR using M13 primers. Synthesis of digoxigenin (DIG)-labeled antisense riboprobes was performed with a DIG RNA Labeling Mix (Roche, #11 277 073 910) and T3 or T7 RNA polymerase (depending on insert orientation, Roche, #11 031 163 001 & #10 881 767 001) as specified in the manufacturer's protocol. Riboprobes were suspended in RNase-free water (20–35 μl) and, after concentration measurement, diluted 1:10 in hybridization buffer (Hyb; 50% deionized formamide [Invitrogen, #AM9342], 5× SSC [0.75 M NaCl, 75 mM $Na_3C_6H_5O_7$], 0.1% Tween-20, 50 μg/ml yeast tRNA, 50 μg/ml heparin) and stored at −80˚C until further use.

2.6 | In situ hybridization

After rehydration and transfer into phosphate-buffered saline (PBS; 1.86 mM NaH_2PO_4, 8.41 mM Na_2HPO_4, 17.5 mM NaCl; pH 7.4) at RT, embryos were exposed to Proteinase K (Invitrogen, #AM2546, 20 μg/ml in PBS) for 15 min, followed by three quick rinses in PBS, postfixation in PFA/PBS for 20 min, and thorough washing in PBS + 0.1% Tween-20 (PBTw). Next, samples were rinsed in RNase-free water for 5 min and acetylated in TEA solution (0.1 M triethanolamine, pH 7.0, freshly supplemented with 0.25% [v/v] acetic anhydride) for 20 min, followed by thorough washing in PBTw, incubation in Hyb-Wash1 buffer (Hyb-W1; 50% deionized formamide, 5× SSC, 0.1% Tween-20) for 30 min at RT, and prehybridization in Hyb for at least 3–4 h in a water bath at 60˚C. The last step was occasionally extended overnight. While the water bath was heated up to 65˚C, riboprobes were diluted in Hyb, denatured for 10 min at 85˚C, immediately placed on ice for 5–10 min, prewarmed to 65˚C, and exchanged with the prehybridization buffer. Hybridization lasted between 20 and 25 h. Samples were washed at 65˚C in Hyb-W1 (1 × 15 min, 1 × 60 min), Hyb-Wash2 buffer (same as Hyb-W1 but for 2× SSC; 1 × 30 min), 2× SSC + 0.1% Tween 20 (1 × 20 min), and 0.2× SSC + 0.1% Tween 20 (3 × 20 min) and subsequently transferred to RT.

For colorimetric detection of gene expression, samples were rinsed in PBTw (3 × 5 min or more) and incubated in blocking buffer (0.1 M maleic acid, 0.15 M NaCl, pH 7.5,

containing 1% [w/v] blocking reagent [Roche, #11 096 176 001]) for 2 × 1 h at RT, followed by application of alkaline phosphatase-conjugated anti-DIG Fab fragments (sheep, Roche, #11 093 274 910, 1:2000 in blocking buffer) overnight at 4˚C. Samples were brought back to RT, washed in PBTw for several hours, equilibrated in freshly prepared AP buffer (100 mM NaCl, 5 mM $MgCl_2$, 100 mM Tris–HCl, 0.1% Tween-20, pH 9.5) for 2 × 10–15 min, and incubated in 1-Step™ NBT/BCIP substrate solution (Thermo Scientific, #34042) in the dark with gentle shaking. Samples were checked at regular intervals (every 15 min, if slow reaction every 30 min) for staining intensity, and the reaction finally stopped in several changes of PBTw. Prior to further processing, samples were transferred into methanol via a graded series and stored overnight at 4˚C.

For fluorescent in situ hybridization (FISH), a TSA® Plus Cy3 fluorescence kit was used (PerkinElmer, #NEL744001KT), with slight modifications to the manufacturer's protocol. Samples were rinsed in TNT buffer (0.1 M Tris–HCl [pH 7.5], 0.15 M NaCl, 0.1% Tween-20; 3 × 5 min or more) and incubated in TNB blocking buffer (TNT buffer with 0.5% [w/v] TSA® blocking reagent [PerkinElmer, #FP1012]) for 2 × 1 h at RT, followed by application of horseradish-peroxidase-conjugated anti-DIG Fab fragments (sheep, Roche, #11 207 733 910, 1:150 in TNB) overnight at 4˚C. Samples were washed in TNT for several hours at RT, equilibrated for several minutes in Amplification Diluent (PerkinElmer, provided in TSA Plus kit), and incubated in the staining solution (Cy3-tyramide stock:amplification diluent at 1:125) for 2–3 h in the dark at RT. To stop the reaction, samples were washed in numerous changes of TNT and repeatedly checked under a fluorescence stereomicroscope to assess whether unbound labeling reagent continued to diffuse from the embryonic yolk reserves.

2.7 | Immunohistochemistry and fluorescent histochemistry

Embryos were rinsed in several changes of PBS at RT and subsequently permeabilized with several changes of PBS + 0.3% Triton-X (PBTx) for ≥2 h. All applied primary and secondary antibodies/-sera were diluted in PBTx; incubation times lasted 24–72 h at 4˚C and were followed by rinsing in PBTx for at least 4 h at RT with gentle agitation on a horizontal shaker and occasional extension overnight at 4˚C.

Acetylated α-tubulin was immunolabeled with a monoclonal primary antibody (mouse, IgG 2b Isotype, clone 6–11 B-1, Sigma–Aldrich #T6793, RRID: AB_477585, dilution 1:200) coupled to a Alexa Fluor®647-conjugated secondary antiserum (goat anti-mouse IgG [H+L], Jackson ImmunoResearch Labs #115-605-166, RRID: AB_2338914, dilution 1:200). This allowed visualization of cell shapes and neurite bundles in the developing nervous system.

Engrailed/invected-positive cells were detected with a monoclonal primary antibody (mouse, clone 4D9, concentrate, DSHB, RRID: AB_528224, dilution 1:100) and an Alexa Fluor®594-conjugated secondary antiserum (goat anti-mouse IgG [H+L], Invitrogen Molecular Probes® #A11062, RRID: AB_2534109, dilution 1:250-300).

The fluorescent nucleic acid marker Sytox™ Green (Invitrogen Molecular Probes® #S7020, 1:1000–2000 in PBS) was applied after all other labeling procedures. Incubation lasted at least 2 h at RT and was occasionally extended overnight at 4˚C.

2.8 | Mounting of samples

Complete embryos (whole mounts) were transferred into a petri dish with a bottom layer of hardened 5% agarose covered by a top layer of PBS. A circular groove (diameter slightly smaller than embryos) was used to hold and orient the samples for stereomicroscopic documentation.

For flat preparations, extraembryonic tissues and yolk were carefully removed with sharpened forceps and insect pins. The embryos were transferred into non-hardening Vectashield® Mounting Medium (Vector Laboratories, Inc. #H-1000, RRID: AB_2336789) and placed on microscopic slides, ventral side facing upward. To permit a direct view on the ventral side of the posterior ETs and newly forming segments, the caudal papilla had to be flipped backward prior to cover slip application. Tiny pieces of Surgident periphery wax attached to the corners of the cover slip acted as flexible spacers that were gradually pressed under a stereomicroscope to avoid compression of the samples by the cover slip.

2.9 | Data documentation, analysis, and presentation

Brightfield and epifluorescence images of complete embryos were taken with a Nikon SMZ25 stereomicroscope, equipped with a Nikon DSRi2 camera. Z-stacks were generated and combined into an image with extended depth of field with the complementary NIS Elements AR software (ver. 4.51, Nikon Corporation, Tokyo, Japan, RRID: SCR_014329).

Flat preparations were documented with a Nikon Eclipse 90i epifluorescence microscope, equipped with a Nikon DS Fi3 camera. *XY*-tiling, acquisition of multichannel Z-stacks, and combination into images with extended depth of field were in most cases managed in the accompanying NIS Elements AR software (ver. 5.02, Nikon Corporation). Z-stack merging for higher resolution images was performed

with Helicon Focus (ver. 7.6.6, Helicon Soft Ltd., Kharkiv, Ukraine, RRID: SCR_014462)

Confocal laser scanning microscopy (CLSM) was performed with a Leica DMI 6000 CS microscope coupled to a Leica TCS SP5 II scan unit (RRID: SCR_018714). Laser lines were chosen according to the excitation spectra of the fluorochromes used (488 nm argon laser → Sytox™ Green; 543 nm helium–neon laser → Cy3 & Alexa Fluor® 594; 633 nm helium–neon laser → Alexa Fluor® 647). The Z-increment between optical planes ranged between 0.80 and 2.00 μm, depending on the objective used and required resolution.

The three-dimensional reconstruction software Imaris (ver. 7.00; Bitplane AG, Zurich, Switzerland, RRID: SCR_007370) was used for CLSM data analysis. Software tools were applied as previously described (Brenneis et al., 2013; Brenneis & Beltz, 2020). Global contrast and brightness of images were adjusted using Adobe Photoshop (ver. 12.1, Adobe Systems Incorporated, San Jose, CA, USA, RRID: SCR_014199). All figures were compiled with Adobe Illustrator (ver. 15.1, Adobe Systems Incorporated, RRID:SCR_010279).

3 | RESULTS

3.1 | Target genes and phylogenetic analyses of *SoxB* group, *achaete–scute* complex, and *Snail* family TFs

BLAST searches yielded single copies of the two potential neural differentiation factors *Prospero* (*Pv_Pros*) and *Brain tumor* (*Pv_Brat*) and of the neuron marker *Embryonic lethal abnormal visual system* (*Pv_Elav*).

Candidate sequences of the three target *SoxB* group genes *SoxNeuro* (*Pv_SoxN*), *Dichaete* (*Pv_D*), and *Sox21b* (*Pv_Sox21b*) were identified. Based on the scaffolds of the *P. virginalis* draft genome, *Pv_D* represents a single intronless transcription unit (scaffold 36382), whereas *Pv_Sox21b* contains at least two introns, one of which is located inside the HMG domain (scaffold 134090). In validation of our assignment of the three *P. virginalis* genes to the *SoxB* group, they cluster together with the *SoxB* members in the phylogenetic analysis of the HMG boxes of *Sox* groups B–F in other arthropods (Figure S1a). Within this well-supported *SoxB* lineage (PP = 1), the *SoxNeuro* orthologs are recovered as a moderately supported monophyletic group (PP = 0.87) that is nested within a poorly resolved paraphyletic assemblage composed of the *Dichaete*, *Sox21a*, and *Sox21b* members in no gene-specific order. *Pv_SoxN* and *Pv_D* are closely related to the respective orthologs of the decapod crustacean *M. nipponense*, whereas *Pv_Sox21b* groups with *Dichaete* of the millipede *Glomeris marginata* and *Pv_Sox21b* of *M. nipponense*. However, in all three cases, these groupings lack support (PP < 0.7).

Two *achaete–scute* complex genes (*Pv_ASH1* and *Pv_ASH2*) were identified for *P. virginalis*. The arthropod-wide phylogenetic analyses of the bHLH domain alone and in conjunction with the C-terminal motif result in poorly resolved topologies for the different *achaete–scute* complex members with overall low support values. In the latter analysis, *Pv_ASH1* is recovered (PP = 0.99) as closely related to the single *ASH* gene hitherto known in the spiny lobster *Panulirus argus* (Chien et al., 2009) and these cluster in turn with the two *ASH* genes we identified in the amphipod *Parhyale hawaiensis* (PP = 0.99) (Figure S1b).

Three members of the *Snail* TF family were identified (*Pv_Sna1*, *Pv_Sna2*, and *Pv_Sna3*). In the analysis of the five zinc-finger domains of the arthropod *Snail* superfamily genes, the *Snail* TFs of *P. virginalis* and all other malacostracan crustaceans studied (dendrobranchiate *Penaeus* ssp. and the amphipod *P. hawaiensis*) group together (PP = 1.00) (Figure S2). Notably, this well-supported monophyletic group also contains *Drosophila snail*, but neither the two other *Drosophila Snail* family members *worniu* and *escargot*, nor any other insect *Snail* TF. Further, the *Snail* TFs of *P. virginalis* and the amphipod *P. hawaiensis* form separate clades (PP = 0.86 and PP = 1.00, respectively). In our gene expression experiments, only *Pv_Sna1* was studied in more detail, as preliminary experiments indicated its expression in the early NE and in later stages of CNS development.

3.2 | General observations on the quality of gene expression patterns

From stage 4 onward, the secretion of embryonic cuticle near the developing carapace rim and in the area of the invaginating stomodeum leads to nonspecific probe binding. However, the resulting homogeneous surface staining could be readily differentiated from specific gene expression in the ectoderm. Further, the yolk reorganization during stages 3 and 4 (see Alwes & Scholtz, 2006) leads to a cavity filled with amorphous yolk underlying the posterior pole in whole mount embryos. This cavity exhibits diffuse nonspecific labeling, which in case of low gene expression levels made pattern identification more challenging, but comparison of repeated labeling motifs across specimens enabled reliable identification of the gene expression signal. Due to the increasing differentiation of embryonic cuticle in more advanced embryonic stages, expression pattern analyses were restricted to embryonic stages 2–5, and only in exceptional cases extend to stage 7.

Although expression of the candidate neuron marker *Pv_Elav* begins later than that of the remaining genes studied, it is in the following presented directly after the *SoxB*

group genes. This order was chosen to highlight the largely complementary expression domains of both gene classes and to visualize the maturating neuronal structures in the different stages prior to description of further genes involved in their formation.

3.3 | Expression of *Pv_SoxN*

In stage 2, *Pv_SoxN* is expressed in a V-shaped domain that extends over parts of the optic lobe and naupliar segmental anlagen (Figures 2a,b and 3a). Expression is widest in the optic lobe, where it covers a central field, which has a sharp border with the midline-spanning cell regions and does not reach into the lobe's anterolateral portion (Figure 2a). Tubulin immunolabeling reveals apically converging processes of flask-shaped cells and cell groups with basally displaced nuclei scattered across the otherwise single-layered lobe, indicative of the beginning of neuroectodermal cell emigration (Figure 2c–e). Cells emigrating from the apical *Pv_SoxN*-expressing domain retain expression of this TF (Figure 2d,e). In each of the naupliar segments, expression occurs in a central patch that covers the NE but more laterally also in cells that may later become involved in the formation of the limb buds. Only at the posterior margin of the mandibular segment, expression is contiguous between the body halves (Figure 2a,b,f). Cell division patterns on both sides of the posterior expression border do not differ markedly; in both cases, they are characterized by mitotic profiles with tangential orientation (Figure 2f). There are no signs of larger, radially dividing cells (putative NBs) in any part of the embryo. The incipient caudal papilla, which includes the first forming ETs, lacks expression of *Pv_SoxN* (Figures 2b and 3a).

During stage 3, *Pv_SoxN* continues to be strongly expressed in the thickened V-shaped naupliar NE (Figure 3b). The optic lobe has become multilayered and attained an oval shape (Figure 3b,c). Apically, it features some cells that are slightly enlarged. At its medial margin, a population of *Pv_SoxN*-expressing cells is set off from more lateral areas, resembling the first demarcation of the median and lateral protocerebral brain areas (Figure 3b,c). In early stage 3, only single cells directly posterior to the mandibular NE have initiated expression, but only slightly later, it begins to extend next to the ventral midline into the maxilla 1 ectoderm (Figure 3c). The first telson cells posterior to the *Pv_SoxN*-negative ETs show expression (Figure 3c).

Toward stage 4, the maxilla 1 and maxilla 2 segments display distinct expression along the midline and its two adjacent cell columns (Figure 3d). The optic lobe continues to show ubiquitous expression, except for a central area composed of a few cells with small nuclei. In parallel with the outgrowth of the labral anlage, the ectodermal *Pv_SoxN* domain becomes narrower in the antenna 1 and 2 segments. Medially only a few cells feature elevated expression levels, likely related to stomatogastric nervous system development (Figure 3d). Distally in antenna 2, a group of cells has started to express *Pv_SoxN*.

In stage 5, *Pv_SoxN* expression extends from the optic lobe along the entire NE into the caudal papilla, where it stops at a sharp transverse border (Figures 4a–c and 5a,b). Further, the entire telson anlage shows moderate expression levels (Figures 4b,c). In the limb buds, *Pv_SoxN* is upregulated in a distal domain, located at the (prospective) branching point of exo- and endopodites in biramous limbs (Figure 4a,c). Only the mandible lacks this domain; expression occurs instead in its proximal gnathobasic part (Figure 4a). For more details at cellular level, tubulin immunolabeling was combined with FISH. At this point, major axonal pathways of the circumoral embryonic brain have already been established in the naupliar region, including the preoral commissure in the prospective median protocerebrum and the protocerebral tract connecting it to the lateral protocerebrum in the optic lobe (Figure 5a). The distal rim of the optic lobe, in which the ommatidia will develop, stays *Pv_SoxN* negative (Figures 4a and 5a). In the apical cell layer proximal to this rim, expression forms a ring that surrounds a central nonexpressing patch and is medially and posteriorly contiguous with the median protocerebrum and naupliar NE, respectively (Figures 4a and 5b). Transverse and horizontal sections reveal this ring-like domain represents a multilayered proliferative region housing cells with comparatively large nuclei and numerous mitotic profiles (Figure 5c,d), characteristic for neural progenitors and their mitotically active progeny. The proliferative region envelops the nonexpressing differentiating neurons, into which the protocerebral tract is embedded (Figure 5c,d). In the naupliar and postnaupliar NE, the apical NBs are *Pv_SoxN* positive and continue to display elevated transcript levels during their asymmetrical radial divisions (Figures 4a and 5e–g). Expression persists also in the subapical cell layer that houses the GMCs, whereas cells in more basal layers of the ganglionic anlagen are *Pv_SoxN* negative (Figure 5f,g).

During segment differentiation in the caudal papilla, the posterior expression border aligns with genealogical units rather than with the future morphological segment borders. The posterior-most *Pv_SoxN*-positive cells along the midline and cell columns 1 and 2 belong to row d (Figures 1d and 4b,c). Occasionally, we observed the onset of first differential cleavages in the ultimate *Pv_SoxN*-positive d-row, whereas the cells of the posteriorly adjacent genealogical unit still lacked *Pv_SoxN* signal (Figure 5h,i). This points to coordinated upregulation of expression within each genealogical unit, falling between the second mitotic wave and the initiation of the differential cleavages. During these early phases of segment formation, expression is strictly confined to the single-layered apical ectoderm (Figure 5j).

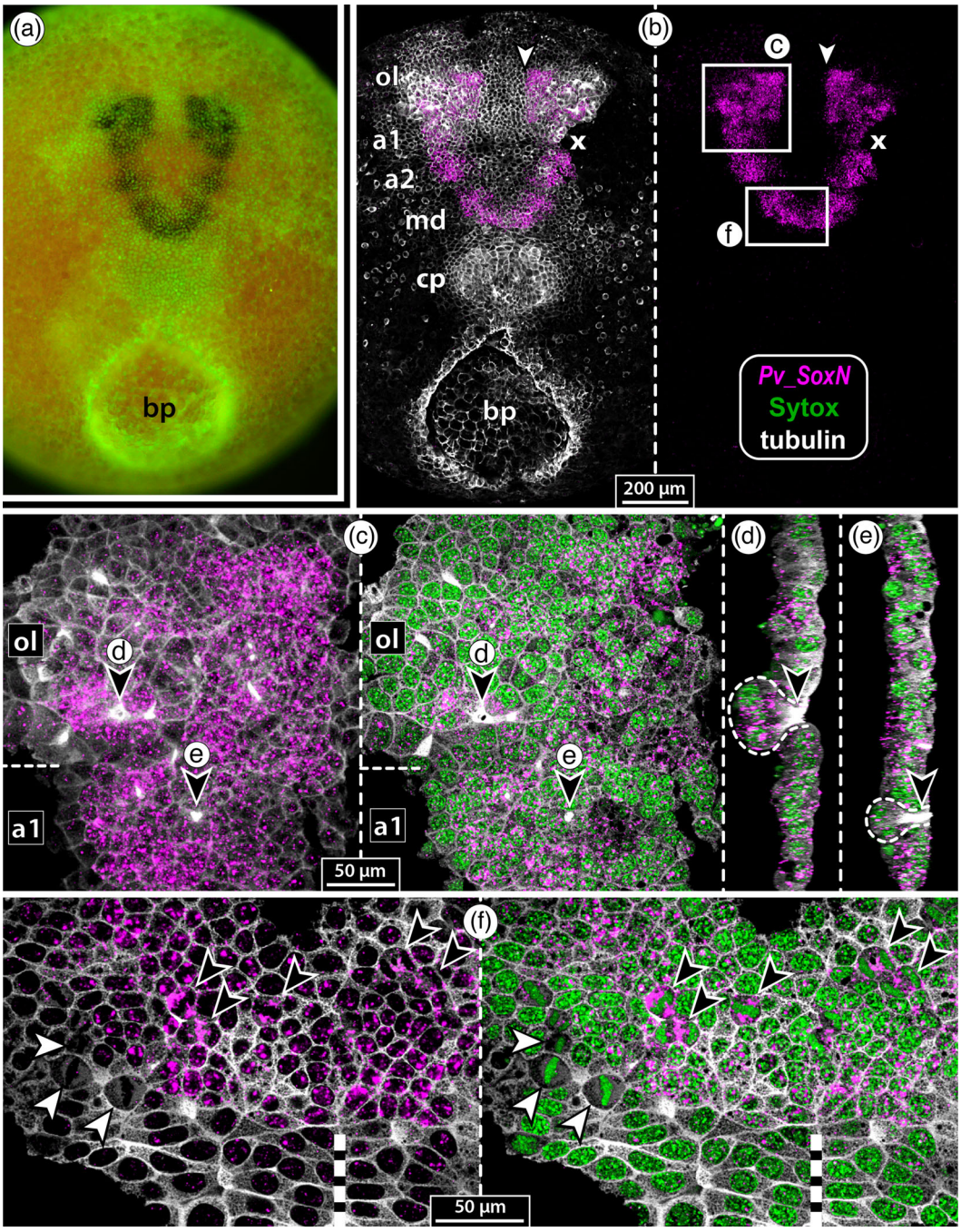

FIGURE 2 *Pv_SoxN* expression in stage 2. (a) Ventral overview. Colorimetric *Pv_SoxN* detection (dark blue) with Sytox nuclear counterstain (green), stereomicroscopic micrograph. Note large circular blastopore posterior to the embryo. (b–f) CLSM scans of *Pv_SoxN* FISH (magenta) with tubulin immunolabeling (white) and Sytox nuclear counterstain (green). (b) Ventral overview. The incipient caudal papilla and blastopore are devoid of expression. The arrowhead points to the sharp medial expression border in the optic lobe. The "x" marks a damaged region of the embryo. Rectangles highlight areas magnified in panels (c) and (f). (c) Detail of optic lobe and antenna 1 NE. Maximum-intensity projection in ventral view (left) and optical section through the same area (right). Note tubulin-labeled apically converging cell processes. (d and e) Longitudinal optical sections at the levels indicated by arrowheads in panel (c). (d) A conspicuous group of *Pv_SoxN*-expressing cells (arrowhead) emigrates from the apical ectoderm of the optic lobe into a subapical position. (e) A small group of *Pv_SoxN*-expressing cells (arrowhead) emigrates from the antenna 1 NE. (f) Horizontal optical section through mandibular NE. Note multiple *Pv_SoxN*-positive mitotic profiles with tangential orientation (black arrowheads) in the NE and *Pv_SoxN*-negative mitotic profiles in adjacent ectoderm (white arrowheads). Abbreviations: a1 and a2, antenna1 and 2 segments; bp, blastopore; cp, caudal papilla; md, mandibular segment; ol, optic lobe

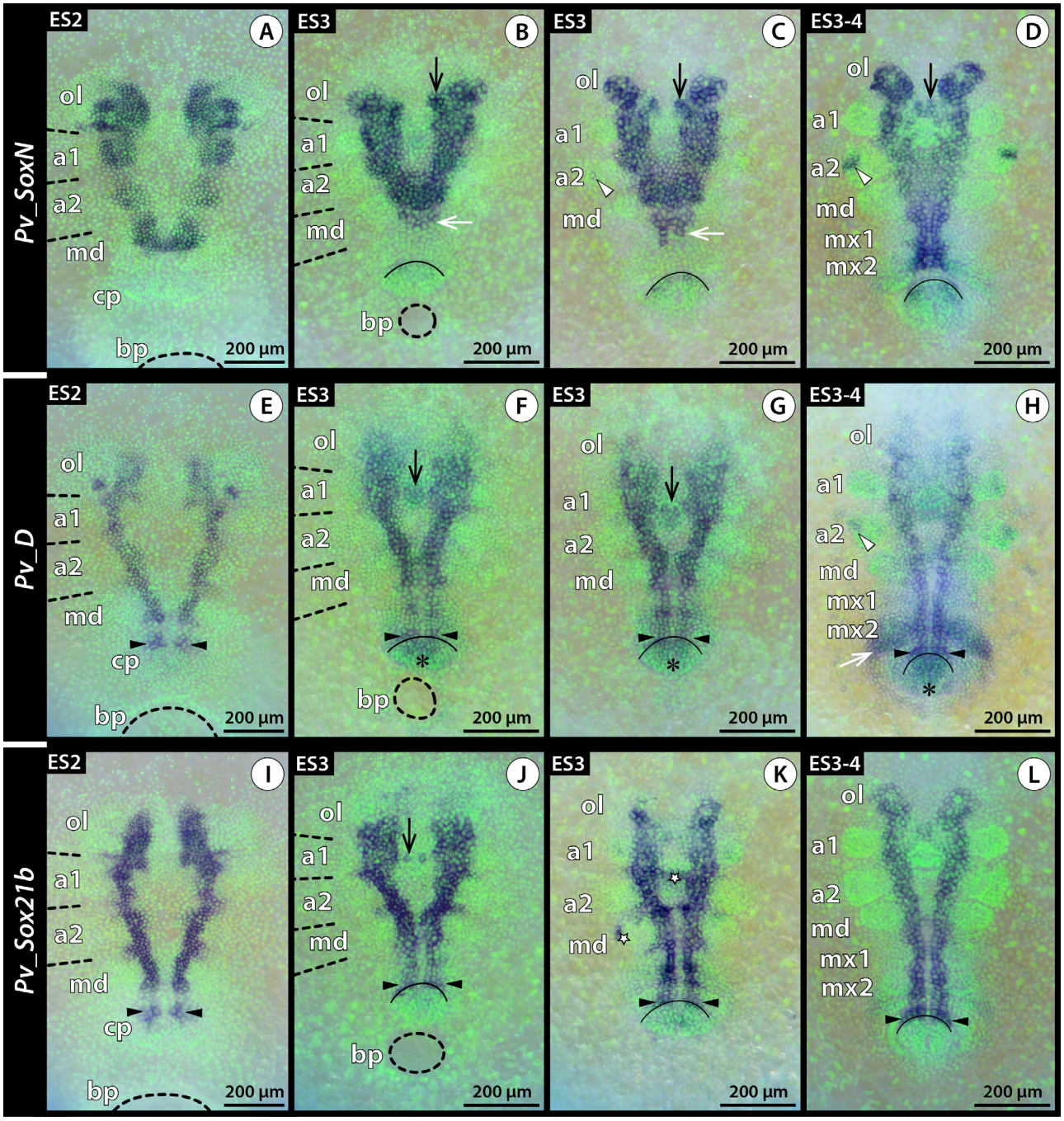

FIGURE 3 Expression of *Pv_SoxB* group genes in stages 2–4. Ventral views of colorimetric whole mount ISH (dark blue) with Sytox nuclear counterstain (green), stereomicroscopic micrographs. Black curved lines are drawn behind the developing ring of ETs. Stippled crescents and ovals mark the blastopore (bp). (a–d) *Pv_SoxN* expression. Note condensation of naupliar NE as the naupliar region compacts between stages 2 and 3. In stage 3, an anteromedial protocerebral expression domain (black arrows) becomes distinct from the optic lobe (ol). In the postnaupliar NE of stage 3, first expression begins and extends into successively more posterior segmental anlagen (white arrows). Toward stage 4, antenna 2 (a2) displays a distal expression domain (white arrowheads). (e–h) *Pv_D* expression. Asterisks mark the location of the developing proctodeum; black arrows point to the site of stomodeum development. Black arrowheads highlight *Pv_D*-expressing ETs 1–3. In the naupliar region of stages 2 and 3, note more restricted lateral extension of expression compared to *Pv_SoxN*. Toward stage 4, single cells in the naupliar limb buds (a1, a2, md) display expression (white arrowhead). The early segmental anlagen of maxilla 2 (mx2) and maxilliped 1 (white arrow) show broad expression along their entire mediolateral extension. (i–l) *Pv_Sox21b* expression. Note similarity to *Pv_D* expression in the NE, but stronger signal intensity in the optic lobe. Black arrowheads highlight *Pv_D*-expressing ETs 1–4. A single cell in the region of the developing stomodeum is labeled (black arrow). Stars mark nonspecific surface labeling. Abbreviations: a1 and a2, antenna 1 and 2 segments; bp, blastopore; cp, caudal papilla; md, mandibular segment; mx1 and mx2, maxilla 1 and 2 segments; ol, optic lobe

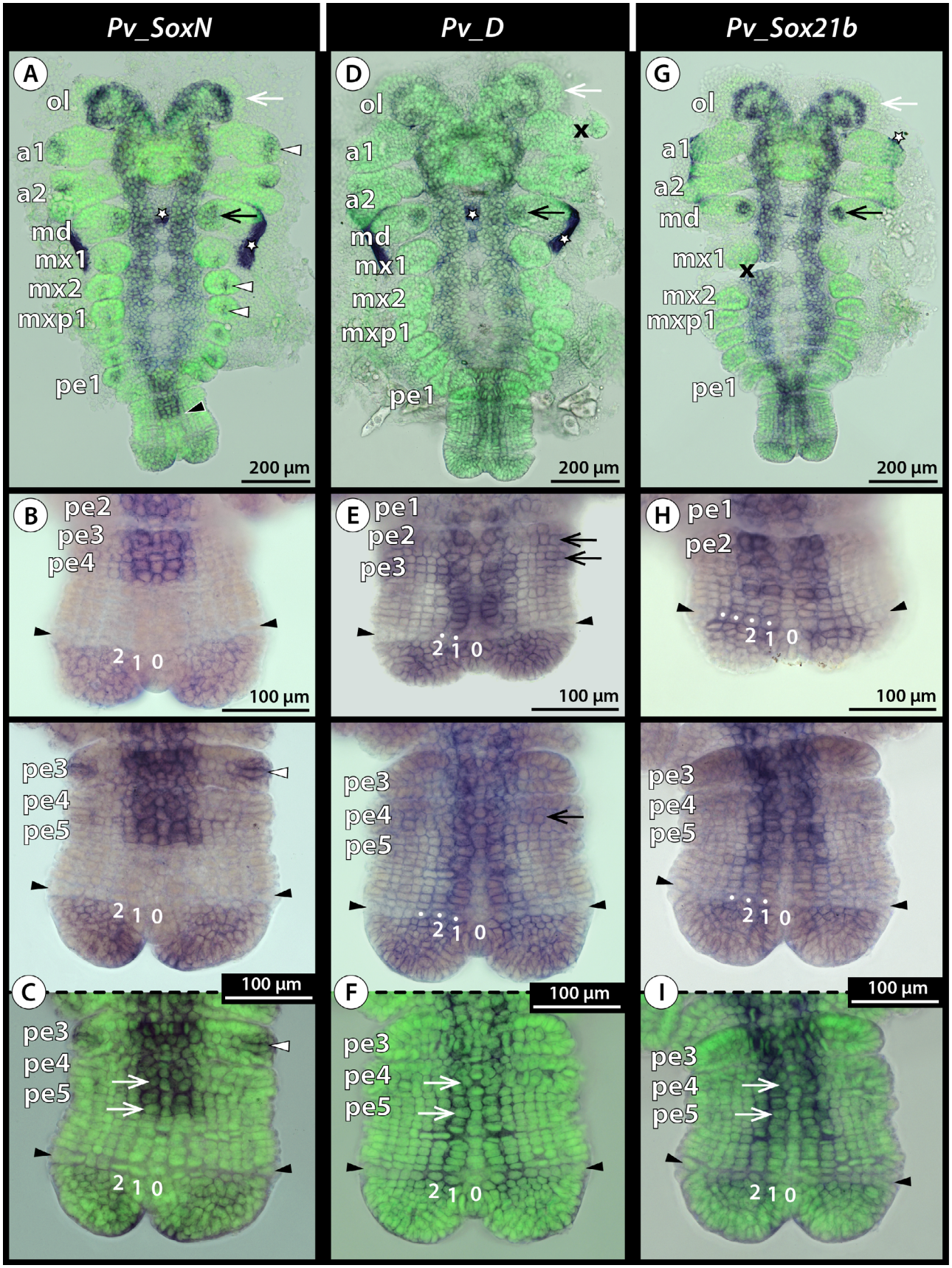

FIGURE 4 Expression of *Pv_SoxB* group genes in stage 5. Flat preparations of colorimetric ISH (dark blue) with Sytox nuclear counterstain (green), light microscopic micrographs. Stars mark nonspecific surface labeling of developing cuticle. "x" marks damaged tissue. White dots

3.4 | Expression of *Pv_D* and *Pv_Sox21b*

Expression patterns of *Pv_Sox21b* were more distinct than those of *Pv_D*, as the latter were more susceptible to background labeling. Regardless of this issue, both *SoxB* group TFs displayed considerable similarities in their expression domains.

In stage 2, *Pv_D* and *Pv_Sox21b* are expressed along a longitudinal band reaching from the optic lobe to the mandibular segmental anlage without crossing the midline (Figure 3e,i). The band is narrower than the *Pv_SoxN* expression domain (compare Figure 3a) and overlaps only with its medial portion. In the optic lobe, an additional lateral cell group expresses *Pv_D* and *Pv_Sox21b*, corresponding to a site of cell emigration identified in the *Pv_SoxN* experiments (Figure 2c,d). Further, both genes are expressed in some cells of the early caudal papilla, including the first ETs of columns 1–3, but not ET0 of the midline (Figure 3e,i).

In stage 3, expression in the naupliar region is more similar to *Pv_SoxN*. In contrast to the latter, *Pv_D* is only relatively weakly expressed in the optic lobe (compare Figures 3b and 3f). Further, it is upregulated in a median cell group between the NE of antennae 1 and 2, coinciding with the onset of stomodeum development in this area (Figure 3f,g). In the same area, *Pv_Sox21b* is found in a single cell only, which may relate to the development of stomatogastric nervous system elements in the stomodeal wall (Figure 3j). In the postnaupliar region, both genes are expressed in neuroectodermal cell columns 1 and 2, but still not along the midline (Figure 3f,g,j,k). The ETs of columns 1–3—in some samples even of column 4—express both genes, posteriorly bordered by telson cells with elevated transcript levels. *Pv_D* is additionally expressed in the proctodeal anlage (Figure 3f,g)

Toward stage 4, *Pv_D* expression decreases further in the optic lobe and naupliar NE, except for a few strongly labeled apical cells (presumably NBs) (Figure 3h). *Pv_Sox21b* expression remains distinct and looks very similar to *Pv_SoxN*, including the nonexpressing central cell region in the optic lobe (compare Figures 3d and 3l). Notably, the segmental anlage of maxilliped 1 displays broad *Pv_D* expression in a laterally extending stripe that includes the early limb bud primordium (Figure 3h). Additionally, some cells in the naupliar limb buds are *Pv_D*-positive (Figure 3h). Both regions lack *Pv_Sox21b* signal (Figure 3l).

In stage 5, *Pv_D* and *Pv_Sox21b* are expressed in the ring-shaped proliferative zone of the optic lobe (*Pv_D* only weakly) and along the entire NE (Figure 4d,g). A domain in the gnathobasic part of the mandible shows expression, whereas the limb bud tips are devoid of it (Figure 4d,g). In the caudal papilla, *Pv_D* is weakly expressed in the ETs of columns 1 and 2 (sometimes also of column 3) and displays high transcript levels along cell column 1 and to a lower extent also in column 2 (Figure 4e,f). *Pv_Sox21b* expression covers at least ET1–3, but may include also ET4 (Figure 4h,i). Along cell columns 1 and 2, upregulation of *Pv_Sox21b* occurs slightly later than for *Pv_D*, but prior to the onset of *Pv_SoxN* expression (Figure 4b–i).

3.5 | Expression of *Pv_Elav*

Stage 2 embryos lack distinct expression of *Pv_Elav* (Figure 6a). Unequivocal expression begins in stage 3. Except for a small domain lateral to the proctodeal anlage in the caudal papilla, it remains restricted to the naupliar region until stage 4, extending from the optic lobe's center posteriorly, in line with the NE. Low-resolution stereomicroscopic investigation of whole mount embryos indicates that expression is absent from the apical neuroectodermal cell layer (see next paragraph). In addition, *Pv_Elav* is expressed (1) by a few cells of the median protocerebrum, (2) in single cells in the labral anlage, and (3) along short intersegmental stripes that extend laterally from the NE (Figure 6b).

Until stage 5, the naupliar expression domains have grown in volume and the two hemispheres of the prospective median protocerebrum are interconnected (Figure 6c). In the ganglionic anlagen of the anterior postnaupliar segments, the first cells have initiated expression (Figure 6c). To obtain

highlight ETs featuring (weak) expression. (a, d, and g) Ventral overviews. White arrows point to the expression-free crescent-shaped distal region of the optic lobe. Black arrows mark the expression domain in the gnathobasic portion of the mandible (md). (b, c, e, f, h, and i) Details of the caudal papilla. Black arrowheads indicate the location of the ET ring. Numbers indicate the position of cell columns 0–2. Note weak expression of the three *SoxB* genes in telson cells posterior to the ETs. (a) *Pv_SoxN* displays a sharp expression border in the caudal papilla (black arrowhead). The tips of all limb buds except for the mandible display expression (white arrowheads). (b) Early stage 5 (specimen shown in panel [a]). (c) Advanced stage 5. White arrows point to cell d1 and NB d1h. The limb bud primordia display a small distal expression domain (white arrowhead). (d) Note weaker *Pv_D* expression compared to the other two *SoxB* group genes. (e) Stage 4–5. The ETs of column 1 and 2 are weakly labeled. Note strong *Pv_D* expression in cell column 1 and lower intensity in column 2. After onset of the second mitotic wave, some more lateral cells show weak expression (black arrows). (f) Advanced stage 5. Expression remains strongest in cell column 1. (g) *Pv_Sox21b* expression is very similar to *Pv_D*. (h) Stage 4–5. The ETs of cell columns 1–4 are weakly labeled. Note weak expression in the cells of columns 1–3, with stronger signal intensity in columns 1 and 2 after the onset of the first mitotic wave. (i) Advanced stage 5. Between the first and second mitotic waves, expression becomes strongest in columns 1 and 2. Abbreviations: a1 and a2, antenna 1 and 2 segments; md, mandibular segment; mx1 and mx2, maxilla 1 and 2 segments; mxp1, maxilliped 1 segment; ol, optic lobe; pe1–5, pereiopod 1–5 segments

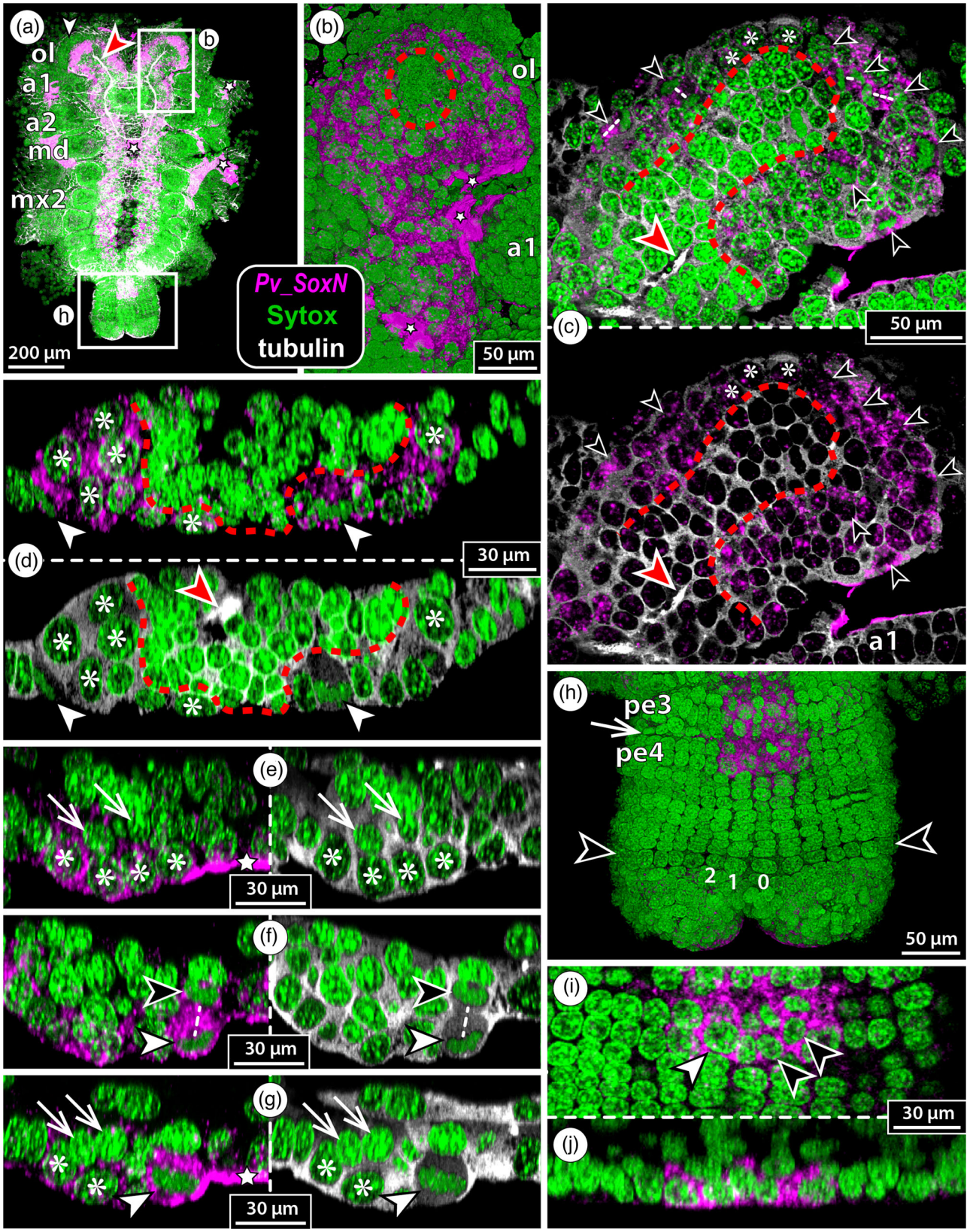

FIGURE 5 Details of *Pv_SoxN* expression in stage 5. FISH (magenta) with tubulin immunolabeling (white) and Sytox nuclear counterstain (green), CLSM scans. Stars mark nonspecific surface labeling of developing cuticle. Asterisks highlight selected NBs in the optic lobe (ol) and ventral NE. The red arrowhead indicates the tract connecting the median protocerebrum and optic lobe. (a) Flat preparation, ventral view. Note the anlage of major axonal pathways of the brain. The white arrowhead marks the *Pv_SoxN*-negative distal rim of the optic lobe. (b) Detail of the area indicated in panel (a) (volume rendering, blend mode). Note *Pv_SoxN* signal in the apical cell layer and the expression-free domain in the optic

additional details at the cellular level, we used tubulin immunolabeling in conjunction with FISH (Figure 6d–j). *Pv_Elav* expression is virtually absent from apical cell layers (Figure 6d,f,j). Neither the multilayered ring-like proliferative region in the optic lobe nor the apically located NBs of the naupliar and postnaupliar segments display expression, irrespective of cell cycle phase (Figure 6d–i). In the optic lobe, expression is restricted to the central area of cell bodies arranged around the protocerebral tract (Figure 6d). This represents a domain complementary to the proliferative region highlighted by the *SoxB* group TFs studied (see Figure 5b–d) and supports predominant expression of *Pv_Elav* in differentiating and mature neurons. Also in the brain neuromeres, expression is concentrated in the neuronal somata surrounding the developing axonal scaffold (Figure 6d). Further, peripheral neurons involved in the formation of the segmental nerves exhibit *Pv_Elav*-positive somata (Figure 6d). In the early ganglionic anlagen of the ventral nerve cord, *Pv_Elav* transcripts become detectable in cells directly subapical to the NBs, indicative of expression prior to terminal division of the GMCs. This is further supported by *Pv_Elav*-positive mitotic profiles in subapical position (Figure 6i). In the caudal papilla, *Pv_Elav* is exclusively expressed in the telson, in the somata of a pioneer neuron cluster with anteriorly projecting neurites that are located lateral to the proctodeum (Figure 6j).

3.6 | Expression of *achaete–scute* homolog 1 (*Pv_ASH1*)

In stage 2, *Pv_ASH1* is expressed in relatively evenly spaced cells and small cell groups across the optic lobe and naupliar NE (Figure 7a). Except for the most lateral cells/cell groups in the optic lobe, expression falls into domains demarcated by at least one of the *SoxB* group TFs studied (see Figure 3a,e,i). The only other exceptions are lateral expression patches in intersegmental position between the three naupliar segments (Figure 7a–a‴). Comparisons among specimens reveals that expression occurs in a pattern of stereotypical sites (Figure 7a–a‴). In different embryos, the same *Pv_ASH1* site may encompass different numbers of cells and/or show deviating expression levels, suggestive of temporally dynamic expression during stage 2 (Figure 7a–a‴). Elevated transcript levels in cell groups are mainly found in the apical cell layer of the NE. However, some stereotypical single cells also show nuclei that are displaced to a subapical position—as ascertained by study of the whole mounts with high magnification stereomicroscopy—and therefore appear slightly unfocused due to overlying apical cells (Figure 7a–a‴). These subapical cells are likely the result of cell emigration from the NE in stage 2. A handful of transversely arranged cells at the posterior border of the mandibular NE show elevated transcript levels (Figure 7a–a‴). In the early caudal papilla, a single cell displays increased expression (Figure 7a–a‴).

In stages 3 and 4, *Pv_ASH1* patterns were more difficult to interpret due to increased overall labeling of the embryonic tissues and the onset of cuticle secretion in the naupliar region. In stage 3, *Pv_ASH1* shows elevated expression in several apical cells or cell duets in the optic lobe and scattered along the naupliar NE (Figure 7b,c). Also, some cells in the naupliar limb buds have started to express *Pv_ASH1*. Further laterally, single cells in intersegmental positions are labeled. Apart from the small domain in the caudal papilla, the postnaupliar region lacks unequivocal expression (Figure 7b,c). In stage 4, *Pv_ASH1* expression has started to extend posteriorly along the postnaupliar NE. At this point, expression in the caudal papilla includes more cells (Figure 7d). Their positions correspond closely to the *Pv_Elav*-positive posterior pioneer neurons (see Figure 6c,j).

In stage 5, expression is found in the optic lobe's proliferative region, while being absent from its semicircular distal rim (Figure 7e,f). In the proliferative region, small cell groups and single cells display higher transcript levels. Neither a strictly stereotypical pattern nor selective upregulation in enlarged cells is recognizable (Figure 7f), speaking against consistently elevated expression in specific neural progenitor cells. In the naupliar and postnaupliar NE, several apical

lobe's center (stippled oval). (c) Curved horizontal section through the optic lobe, shown with and without nuclear counterstain (top and bottom, respectively). The stippled red line outlines the central *Pv_SoxN*-negative region that encompasses the tract to the median protocerebrum. Black arrowheads point to mitotic profiles in the *Pv_SoxN* domain; stippled white lines indicate separating chromosomes in ana- and telophases. (d) Virtual cross section through the optic lobe, shown without tubulin labeling (top) and without *Pv_SoxN* signal (bottom). White arrowheads mark mitotic profiles; asterisks indicate putative large NBs. Note denser packing and smaller cell size in the *Pv_SoxN*-negative central region. (e–g) Virtual transverse sections through the ventral NE of the mandibular to maxilla 2 segmental anlagen. White arrows point to putative GMCs in subapical position. White arrowheads indicate apical NBs undergoing a radial division; black arrowheads mark newly forming GMCs. (h–j) Details of the caudal papilla. (h) Ventral view (volume rendering, blend mode). Black arrowheads highlight the ET ring. Numbers indicate the position of cell columns 0–2. The white arrow points to the forming intersegmental furrow. Note sharp expression border in the segmental anlage of pereiopod 4. (i) Apical horizontal section through segmental anlage pe4. The first differential cleavages have started. At the posterior expression border, d1 has already divided into d1h and d1v (black arrowheads) in the left body half, whereas d1 (white arrowhead) is still undivided in the right body half. (j) Transverse section through segmental anlage of pereiopod 4. Expression is restricted to the single-layered NE. Abbreviations: a1 and a2, antenna 1 and 2 segments; md, mandibular segment; mx2, maxilla 2 segment; ol, optic lobe; pe3 and 4, pereiopod 3 and 4 segments

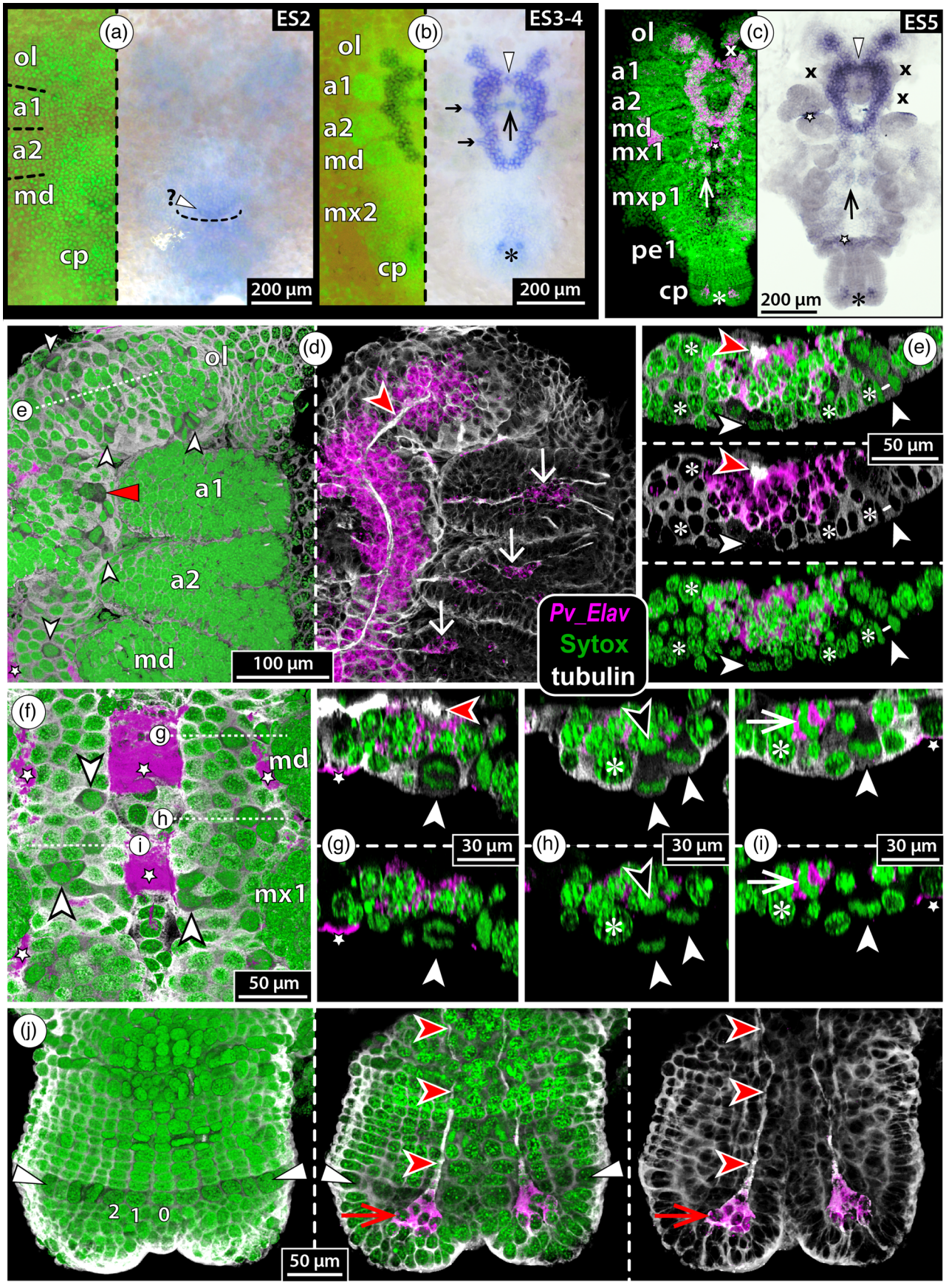
(a)
ES2
ol
a1
a2
md
cp
?
200 µm
(b)
ES3-4
ol
a1
a2
md
mx2
cp
200 µm
(c)
ES5
ol
a1
a2
md
mx1
mxp1
pe1
cp
x
200 µm
(d)
ol
e
a1
a2
md
100 µm
Pv_Elav
Sytox
tubulin
(e)
50 µm
(f)
g
h
i
md
mx1
50 µm
(g)
30 µm
(h)
30 µm
(i)
30 µm
(j)
2 1 0
50 µm

cells are *Pv_ASH1* positive, their number decreasing along the anterior–posterior developmental gradient of the ganglionic anlagen (Figure 7e). Further sites of expression are single cells in the labrum and limb buds as well as along the rim of the developing carapace (Figure 7e,f).

To gain more insight into a potential role of *Pv_ASH1* during NB formation, we scrutinized the expression pattern in the early segmental anlagen of the caudal papilla. Notably, cell d1h—the first NB to differentiate directly anterior to the *engrailed*-positive cell row a of the next genealogical unit—shows distinctly elevated transcript levels (Figure 7e,g). In some specimens, its nonneural sister cell d1v is *Pv_ASH1*-positive as well (Figure 7g). *Pv_ASH1* expression is detected neither in cell d1 of the next younger segmental anlage (giving rise to d1v and d1h with its next division) nor in the next older segmental anlage, in which NB d1h should have started to bud off GMCs (Figure 7g).

3.7 | Expression of *achaete–scute* homolog 2 (*Pv_ASH2*)

Compared to *Pv_ASH1*, signal intensity of *Pv_ASH2* was weaker in our experiments, irrespective of optimization attempts. The expression patterns of both genes differ markedly.

In early stage 2 embryos, fewer than 10 cells show elevated expression centrally in the optic lobe and antenna 1 NE (Figure 8a). Apart from one or two additional cells at the posterior margin of the mandibular NE, the remainder of the naupliar region is devoid of signal. Comparison across specimens reveals a common stereotypical pattern with only marginal differences (Figure 8a–a″). The *Pv_ASH2*-expressing cells are evenly spaced and form a slightly bent grid of two to three short columns and three to four rows. Not every single cell is clearly identifiable in each embryo (Figure 8a–a″), which may be indicative of a spatiotemporal sequence in the upregulation of expression. However, our series of stage 2 embryos is too small to clarify this point. In slightly advanced stage 2, the number of *Pv_ASH2*-positive cells has increased, now also encompassing the first cells in the NE of the antenna 2 segment (Figure 8a″,a‴). Several of the cells are located in sites displaying *Pv_ASH1*-positive cell groups, and in some cases, corresponding positions of single stereotypical *Pv_ASH1*- and *Pv_ASH2*-expressing cells are indicative of co-expression of both genes (Figures 7a–a‴ and 8a″,a‴). Especially in advanced stage 2 embryos, many of the *Pv_ASH2* cells are displaced to a subapical position, resulting in the same unfocused appearance in whole mounts as already noted for subapical *Pv_ASH1* cells (Figures 7a–a‴ and 8a′–a‴).

In the naupliar region of stage 3, elevated *Pv_ASH2* levels are found in single apical cells, but also in cell duets or smaller groups in the optic lobe and NE (Figure 8b,c). The enlargement of several of these cells suggests they may be NBs. Additionally, the incipient stomodeum houses several *Pv_ASH2*-positive cells, as does a domain anterior to and around the proctodeal anlage (Figure 8b,c).

Toward stage 4, expression becomes restricted to fewer cells in the optic lobe and naupliar NE and is slightly upregulated in single cells of the naupliar limb buds (Figure 8d). The postnaupliar NE lacks distinct signal, whereas the early limb

FIGURE 6 *Pv_Elav* expression in stages 2–5. Colorimetric ISH (dark blue) with Sytox nuclear counterstain (green), stereomicroscopic micrographs (a–c), and FISH (magenta) with tubulin immunolabeling (white) and Sytox nuclear counterstain (green), CLSM scans (d–j; left image in panel [c]). Stars mark nonspecific surface labeling of developing cuticle. "x" marks damaged tissue. (a) Stage 2, ventral view. The arrowhead marks a few cells with potential weak expression at the posterior border of the mandibular NE. (b) Stage 3–4, ventral view. The first *Pv_Elav*-expressing cells are found along the midline of the median protocerebrum (white arrowhead) and in the labral anlage (large black arrow). Thin intersegmental stripes extend laterally between the naupliar limb buds (small arrows). The asterisk marks the first expression in the area of the terminal pioneer neurons. (c-j) Stage 5. (c) The median protocerebrum shows a solid midline-spanning domain (white arrowhead). The first cells in the postnaupliar NE have started to express *Pv_Elav* (black arrow). (d) Detail of the naupliar region, left body half, volume rendering in blend mode (left) and maximum-intensity projection with apical clipping planes applied (right). Left image: Note absence of expression in the apical cell layer. White arrowheads mark apical mitotic profiles; the red arrowhead highlights an NB division medial to antenna 1. Right image: Expression is concentrated in neuronal somata surrounding the axonal pathways and in peripheral somata of the segmental nerves (white arrows); the red arrowhead marks the tract between the median protocerebrum and optic lobe. (e) Virtual optical section along the plane indicated in panel (d). Note concentrated expression in the somata around the tract (red arrowhead). Putative NBs (asterisks) and mitotic profiles (white arrowheads) are marked. (f) Detail of the NE in the mandibular and maxilla 1 segments (volume rendering, blend mode). Apart from nonspecific surface labeling on top of the midline cells (stars), the apical cell layer lacks expression. Selected apical mitoses of putative NBs are marked (white arrowheads). (g–i) Transverse optical sections through the ventral NE as indicated in panel (f). Asterisks mark selected NBs. White arrowheads indicate mitotic profiles of radially dividing NBs; the black arrowhead (h) marks the new-forming nucleus of a GMC. Note onset of expression near the basally forming connective (red arrowhead in panel [g]). The white arrowhead (i) points to a dividing subapical cell with strong *Pv_Elav* signal. (j) Detail of the caudal papilla. White arrowheads indicate the ET ring. Note absence of expression in the apical cell layer (left image). Expression is restricted to the posterior pioneer neurons (red arrows in middle and right images, apical clipping plane applied) that project axonal outgrowths anteriorly (red arrowheads). Abbreviations, a1 and a2, antenna 1 and 2 segments; cp, caudal papilla; md, mandibular segment; mx1 and mx2, maxilla 1 and 2 segments; mxp1, maxilliped 1 segment; ol, optic lobe; pe1, pereiopod 1 segment

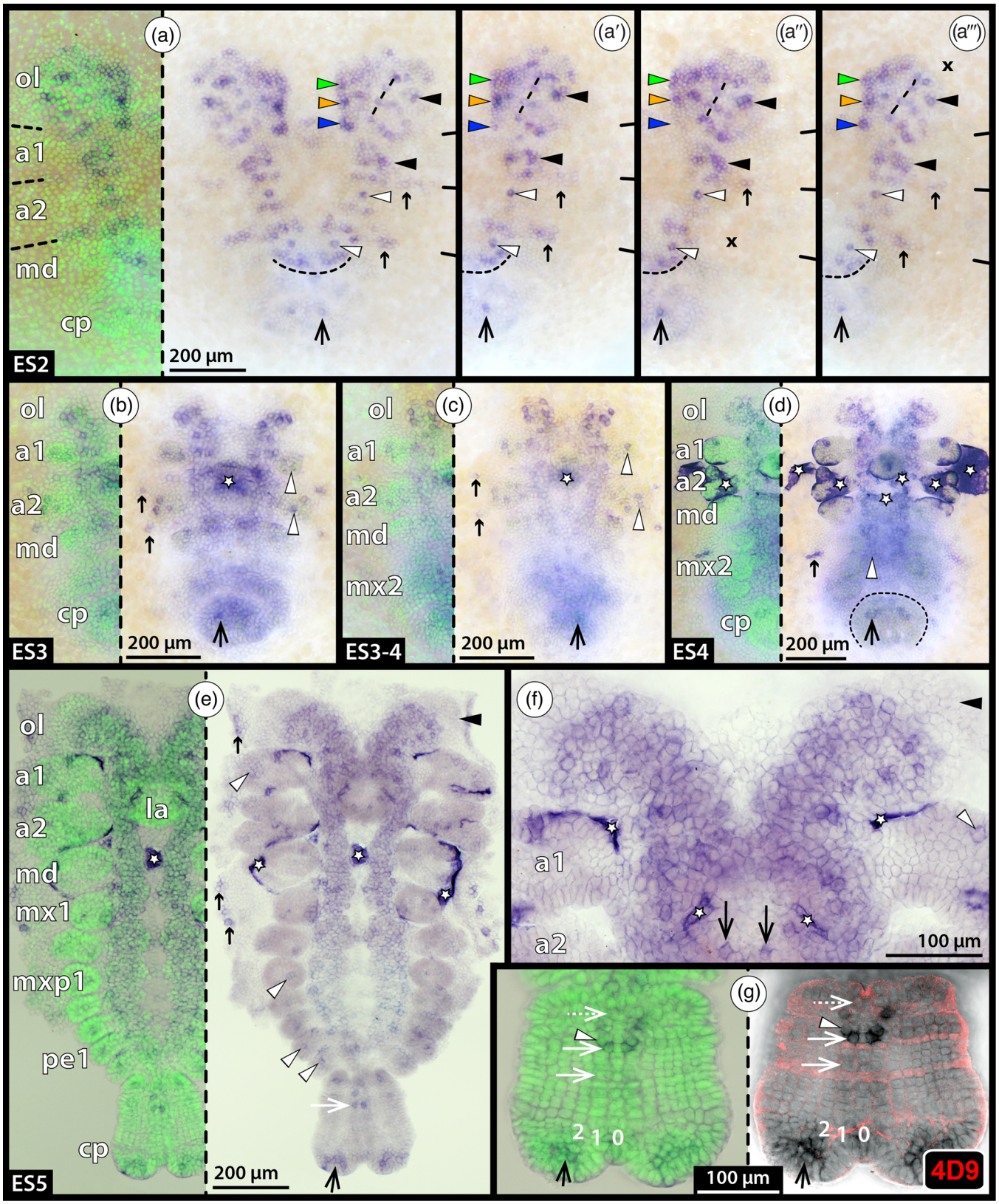

FIGURE 7 *Pv_ASH1* expression in stages 2–5. Colorimetric ISH (dark blue) with Sytox nuclear counterstain (green), ventral view, stereomicroscopic and light microscopic micrographs (a–d and e–g, respectively). Stars mark nonspecific surface labeling. Large black arrows highlight expression in the caudal papilla. (a–a‴) Stage 2. (a′–a‴) The left body half of additional specimens for pattern comparison. Stippled curved lines mark the posterior border of the mandibular NE. The stippled line in the optic lobe spans between corresponding expression sites with partially internalized cells (note milky haze of cytoplasmic labeling due to overlying apical cells). Black and colored arrowheads point to corresponding sites

bud primordia of maxilla 2 and maxilliped 1 display broad, moderate expression (Figure 8d).

In stage 5, three transverse cell bands are found in the NE medial to antenna 1 (Figure 8e–f′). Higher resolution images of the apical layer in this region reveals two to three large *Pv_ASH2*-expressing NBs in each of these bands, being in part surrounded by additional smaller labeled cells (potentially their progeny) (Figure 8f,f′). Also in the optic lobe's proliferative region, several large apical neural progenitors express *Pv_ASH2* (Figure 8f,f′). In the postnaupliar region, the early limb buds and telson show elevated transcript levels (Figure 8e). Notably, in the early segmental anlagen of the caudal papilla, *Pv_ASH2* expression is not upregulated during and after the formation of the first NBs (Figure 8g).

3.8 | Expression of *Pv_Sna1*

In stage 2, *Pv_Sna1* is expressed in a complex pattern of single cells and cell groups in the optic lobe and antenna 1 NE (Figure 9a). With the exception of the anterolateral cells/cell groups, this expression falls in the *SoxB* group expression domains and shows also some overlap with the *Pv_ASH1* pattern (see Figures 3a,e,i and 7a–a‴). The remaining naupliar NE displays only weak expression, which is slightly elevated at the posterior border of the mandibular segment and in single stereotypical cells that also express *Pv_ASH1* and *Pv_ASH2* (Figure 9a; compare Figures 7a–a‴ and 8a″,a‴). In some embryos, short transverse stripes in intersegmental positions also show weak *Pv_Sna1* signal (Figure 9a).

In stage 3, the expression of *Pv_Sna1* is more pervasive in the optic lobe and naupliar NE (Figure 9b). Some neuroectodermal cells display higher signal intensities, but comparison among specimens indicates that expression levels are temporally dynamic and may vary during the cell cycle (see *Pv_Pros* results below). Additionally, *Pv_Sna1* is expressed in (1) a group of median cells at the formation site of stomodeum and labrum, (2) a few cells in the naupliar limb buds, (3) a single cell just distal to the tip of each naupliar limb bud, as well as (4) a single cell proximal to antenna 2 and mandible (Figure 9b). In the postnaupliar region, the posterior edge of the maxilla 1 segment and a cell lateral to the incipient proctodeum exhibit expression.

Toward stage 4, expression persists mainly in the apical layers of the optic lobe and naupliar NE and spreads along the postnaupliar NE, but remains weak along the ventral midline (Figure 9c). The first cells of the developing median protocerebrum are *Pv_Sna1*-positive. Posterior to them, a few cells in the labrum are labeled, potentially related to stomatogastric nervous system development. In the naupliar limb buds, expression extends to several small groups of cells. At the border of the mandibular and maxilla 1 segments, a midline-spanning domain becomes recognizable. Further, a transverse stripe extends from the NE into the limb bud primordia of the maxillae and maxilliped 1.

In stage 5, the proliferative region in the optic lobe is *Pv_Sna1*-labeled, whereas its center and the semicircular distal rim lack expression (Figure 9d,e). Within the proliferative region, apico–basally scattered cells and small cell groups show higher transcript levels, but strictly stereotypical patterns were not apparent. In the median protocerebrum, strong signal is predominantly found in cells in more basal layers (Figure 9e). Most of the naupliar and postnaupliar NE shows expression, including the apical NBs (Figure 9d). Comparison among specimens suggests again temporal dynamics of transcription levels. In the naupliar NE, the NB-containing bands of *Pv_ASH2*-positive cells are encompassed in the *Pv_Sna1* expression domain (Figures 8f,f′ and 9e,e′). The naupliar limbs retain expression in single ectodermal cells or small cell groups, including the gnathobasic part of the mandible, which also features strong *SoxB* group expression at this stage (see Figure 4a,d,g). The midline-spanning domain along the posterior mandibular NE resembles a conspicuous transverse cell

across specimens. Note varying cell numbers and expression intensities in a given site. White arrowheads mark invariant expression in single cells. The small black arrows indicate weak intersegmental expression between the forming naupliar limb buds. (b and c) Stages 3 and 3–4, respectively. White arrowheads mark expression sites in the naupliar limb buds; small black arrows indicate cells in an intersegmental position distal to the limb buds. (d) Stage 4. The first cells in the postnaupliar ventral NE display expression. The curved stippled line outlines the protruding caudal papilla. An intersegmental expression stripe is found between the maxilla 1 and 2 segments. (e–g): Stage 5. (e) Expression extends along the naupliar and postnaupliar NE with a decrease along the anterior–posterior axis. Single cells/cell groups show elevated transcript levels. The distal rim of the optic lobe lacks expression (black arrowhead). Single cells/small cell groups are labeled in the limb buds (white arrowheads) and along the developing carapace (small black arrows). The white arrow points to NB d1h in segmental anlage pe4. (f) Detail of the optic lobes and antenna 1 segment. Note high expression levels in single cells and small cell groups. The black arrowhead highlights the *Pv_ASH1*-negative distal rim of the optic lobe. Single cells are labeled in the labrum (black arrows) and the antenna 1 limb bud (white arrowhead). (g) Detail of the caudal papilla; right image shows a CLSM scan with invected/engrailed immunolabeling (red) to highlight the posterior border of the segmental anlagen. Numbers indicate the position of cell columns 0–2. The white arrows indicate from bottom to top: cell d1 in pereiopod 5 segment, NB d1h in pereiopod 4 segment, and putative NB d1h in pereiopod 3 segment. The arrowhead highlights the *Pv_ASH1*-expressing nonneural cell d1v in the pereiopod 4 segment. Abbreviations: a1 and a2, antenna 1 and 2 segments; cp, caudal papilla; la, labrum; md, mandibular segment; mx1 and mx2, maxilla 1 and 2 segments; mxp1, maxilliped 1 segment; ol, optic lobe; pe1, pereiopod 1 segment

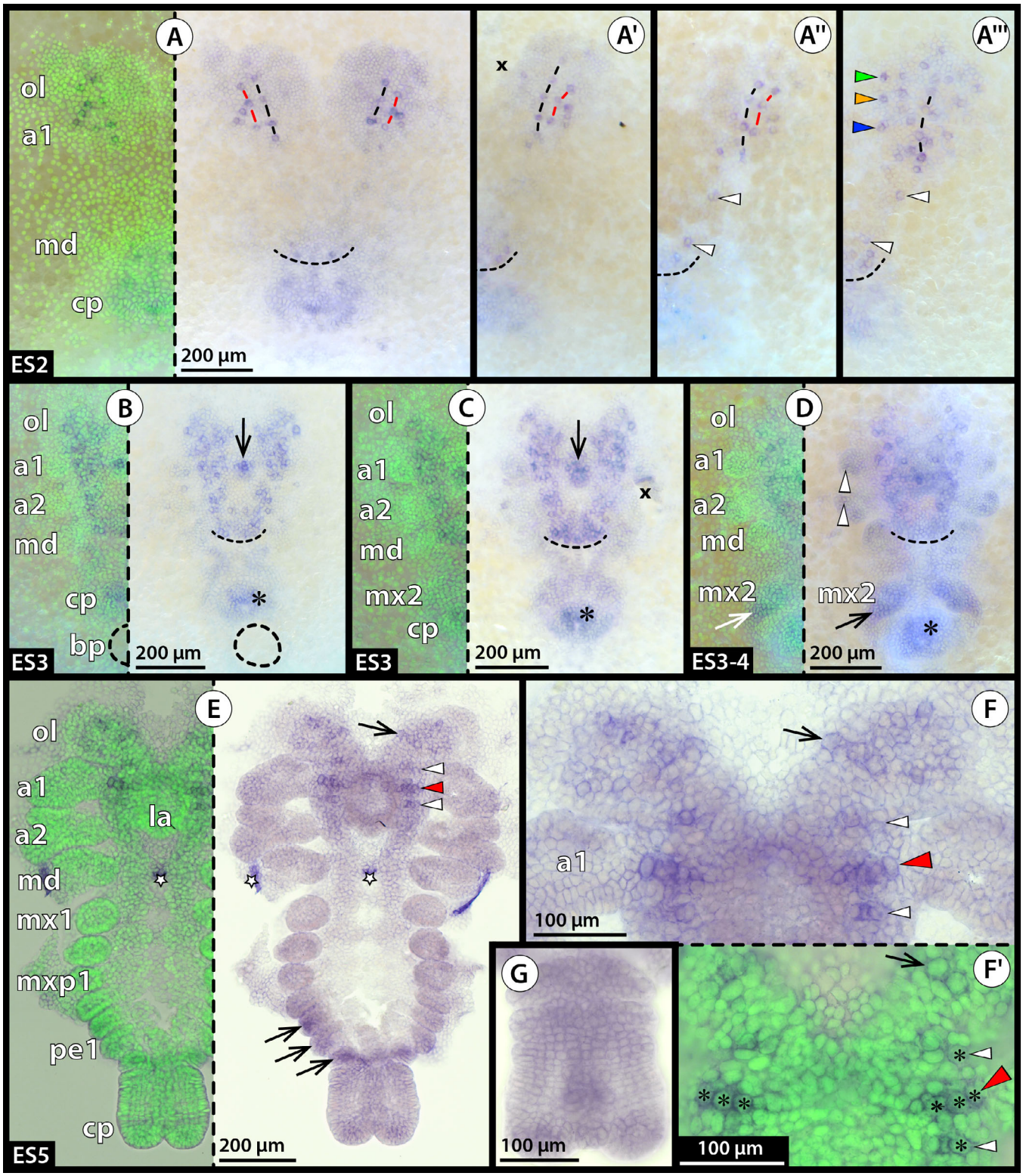

FIGURE 8 *Pv_ASH2* expression in stages 2–5. Colorimetric ISH (dark blue) with Sytox nuclear counterstain (green), ventral view, stereomicroscopic and light microscopic micrographs (a–d and e–g, respectively). Stippled curved lines mark the posterior border of the mandibular NE. Asterisks highlight the expression domain around the proctodeum. Stars mark nonspecific surface labeling. "x" marks damaged tissue. (a–a‴) Stage 2. (a′–a‴) The left body half of additional specimens for pattern comparison. The stippled lines in the optic lobe and antenna 1 segment extend between corresponding single cells. Panel (a) shows an early stage 2 and (a‴) an advanced stage 2 embryo. Note the increase in *Pv_ASH2*-expressing cells and their positional correspondence to *Pv_ASH1*-expressing cells (compare white arrowheads in panels [a″] and [a‴] to Figure 7a–a‴) or *Pv_ASH1* expression sites (compare colored arrowheads in panel [a‴] to Figure 7a–a‴). Note milky haze of the cytoplasmic labeling in several cells

band (Figure 9d). In the postnaupliar segments, a *Pv_Sna1*-expressing strand of ectodermal cells extends from the NE into the limb bud, which additionally displays expression in one or two separate distal cells (Figure 9d). In the caudal papilla, *Pv_Sna1* expression is not restricted to the medial neuroectodermal cell columns but spreads evenly across the entire ventral ectoderm (Figure 9d). Expression sets in around the second mitotic wave of each genealogical unit; the ETs and their youngest progeny are nonexpressing (Figure 9f,f′,g,g′). With further segment differentiation, cell d1 and its daughter, the first NB d1h, also show distinct expression (Figure 9f–g″). Lateral to the proctodeum, single cells are *Pv_Sna1*-positive (Figure 9d). Their position closely matches the *Pv_ASH1*- and *Pv_Elav*-expressing cells in this area (see Figures 6c,j and 7e,g).

3.9 | Expression of *Pv_Pros*

In early stage 2, *Pv_Pros* expression is mainly found in the optic lobe and antenna 1 NE (Figure 10a). In the optic lobe, it is mainly concentrated in the medial portions that are also covered by the *SoxB* TF expression domains (see Figure 3a,e,i). Within the *Pv_Pros* domain, single cells or cell duets are arrayed in a grid-like pattern similar to the pattern of some *Pv_ASH1* cells/cell groups, but even more strikingly to the *Pv_ASH2*-positive cells of stage 2. This correspondence becomes more evident in slightly advanced stage 2 embryos, after *Pv_Pros* expression has spread further across the optic lobe (Figure 10b; compare Figures 7a–a‴ and 8a–a‴). In the naupliar NE, the same stereotypical single cells previously identified in the *Pv_ASH1*, *Pv_ASH2*, and *Pv_Sna1* experiments commence *Pv_Pros* expression and also the posterior margin of the mandibular NE features a small set of labeled cells (Figure 10a,b).

During stage 3, a more compact expression domain is formed in the optic lobe and the remaining naupliar NE features an increasing number of *Pv_Pros*-positive cells. Most of them are in an apical position, presumably including the first forming NBs (Figure 10c,d). Additional expression sites are (1) cells in the region of stomodeum and labrum formation, (2) single cells in the naupliar limb buds, and (3) loosely arranged cell stripes in intersegmental positions (Figure 10c,d). The postnaupliar region lacks signal, except for single or a few cells lateral to the proctodeal anlage (Figure 10d). Around the embryo proper, numerous *Pv_Pros*-positive cells are spread out over the ventral hemisphere; their exact nature is unclear (Figures 10c–e and 11a).

Toward stage 4, the *Pv_Pros* signal in optic lobe and naupliar NE becomes more heterogeneous (Figure 10e). Comparison among specimens suggests expression levels are temporally dynamic at the cellular level. In the postnaupliar segments, the first apical cells have initiated expression in the NE, and lateral to the proctodeum, a few cells are still labeled (Figure 10e).

In stage 5, expression is found in the proliferative region of the optic lobe, whereas the cells in its center are *Pv_Pros*-negative (Figures 10f and 11a). Strong expression extends along the posteriorly adjacent NE, whereas the median protocerebrum shows only comparatively low transcript levels in some specimens (Figure 11a,b). Higher magnification reveals that neuroectodermal expression occurs in densely packed cells of varying sizes and also includes subapical layers (Figure 11b,b′). Medial to antenna 1, the apical NBs previously shown to be *Pv_ASH2*- and *Pv_Sna1*-positive display distinct transcript levels (Figure 11b′; compare Figures 8f,f′ and 9e,f). The naupliar limb buds feature moderate expression in scattered ectodermal cells and small cell groups (Figure 11a,b), including the proximal gnathobasic portion of the mandible. In addition to this, the proximal portion of antenna 2 houses a spherical cluster of *Pv_Pros*-positive cells (Figures 10f and 11a,b), which may be involved in the formation of the antennal gland. Along the postnaupliar NE, the number of *Pv_Pros*-expressing cells decreases from anterior to posterior (Figure 11a). In the neuromeres of the maxillipeds and first pereiopods, expression is restricted to single cells in medial and lateral positions. Also, the limb buds of these segments contain single cells with moderate expression levels (Figure 11a). In addition to the few telson cells, the expression starts to appear first in the older segmental anlagen of the caudal papilla. At this point, they are well into the first differential divisions and have started to bulge outward,

in a subapical position (between stippled lines) due to overlying apical cells. (b and c) Early and slightly advanced stage 3, respectively. Note labeling of scattered apical cells in the optic lobe and naupliar ectoderm. A few cells in the stomodeum (arrow) have initiated expression. (d) Stage 3–4. The number of expressing cells in the naupliar region has decreased. Single cells in the naupliar limb buds are labeled (arrowheads). The limb bud primordia of maxilla 2 and maxilliped 1 (arrow) display expression. (e–g) Stage 5. Red arrowheads mark a *Pv_ASH2*-positive transverse cell row medial to antenna 1. (e) Transverse rows of apical cells are labeled in the optic lobe (single black arrow; see higher magnification in panel [f]) and the proto- and deutocerebral NE (red and white arrowheads). The limb buds anterior to the caudal papilla show an expression domain (black arrows). (f and f′) Details of the anterior head region. The transverse rows of strongly labeled cells (arrow and arrowheads) feature slightly larger nuclei (asterisks in panel [f′]) than most surrounding cells. (g) Detail of the caudal papilla. The ventral ectodermal cells do not show elevated expression levels. Abbreviations: a1 and a2, antenna 1 and 2 segments; bp, blastopore; cp, caudal papilla; la, labrum; md, mandibular segment; mx1 and mx2, maxilla 1 and 2 segments; mxp1, maxilliped 1 segment; ol, optic lobe; pe1, pereiopod 1 segment

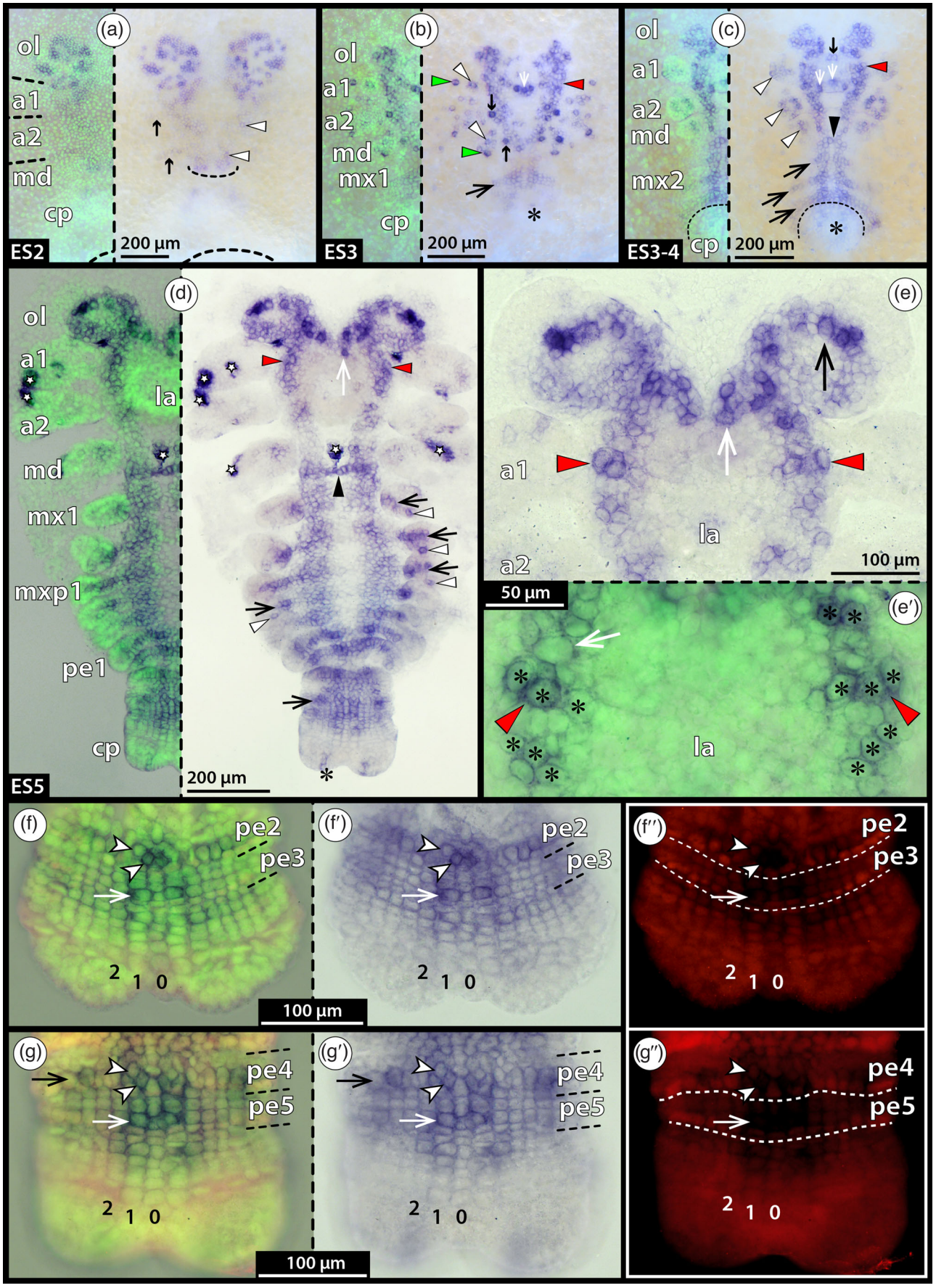
(a)
ol
a1
a2
md
cp
ES2
200 µm
(b)
ol
a1
a2
md
mx1
cp
ES3
200 µm
(c)
ol
a1
a2
md
mx2
cp
ES3-4
200 µm
(d)
ol
a1
a2
md
mx1
mxp1
pe1
cp
la
ES5
200 µm
(e)
a1
la
a2
100 µm
50 µm
(e′)
la
(f)
pe2
pe3
2 1 0
(f′)
pe2
pe3
2 1 0
100 µm
(f″)
pe2
pe3
2 1 0
(g)
pe4
pe5
2 1 0
(g′)
pe4
pe5
2 1 0
100 µm
(g″)
pe4
pe5
2 1 0

flanked by anterior and posterior intersegmental furrows. The first *Pv_Pros*-positive cell is NB d1h, presumably before its first asymmetrical division (i.e., the second differential cleavage) (Figure 11c–c″). Its mother cell d1 and also the newly formed d1h and d1v are devoid of signal, demonstrating that the onset of *Pv_Pros* expression occurs after NB formation (Figure 11c–c″).

Tubulin immunolabeling coupled to FISH further shows that *Pv_Pros* is strongly expressed in NBs as they undergo their asymmetrical divisions: In the caudal papilla of stage 7, which comprises all pleon segmental anlagen, comparably few apical neuroectodermal cells are *Pv_Pros*-positive (Figure 11d). Optical cross sections locate this apical signal in the enlarged NBs, with elevated transcript levels persisting through the different phases of mitosis (Figure 11e–g). Notably, NBs appear to label more strongly in M phase than in interphase (Figure 11e), which may explain at least part of the apparent temporal dynamics noted before. Expression continues in subapical layers comprising the GMCs (Figure 11e), but fades away in the deeper layers that house the differentiated neurons and the first neurite bundles of the major axonal pathways (Figure 11e). Accordingly, *Pv_Pros* is expressed after neural commitment of progenitor cells, but does not persist once cells have differentiated into postmitotic neurons (and glia).

3.10 | Expression of *Pv_Brat*

In stage 2, *Pv_Brat* expression shows notable similarities to the *Pv_Pros* pattern (Figure 12a,b; compare Figure 10a,b). Labeled cells are spread out across the optic lobe and the antenna 1 NE and a pattern reminiscent of a grid-like array is discernible in earlier stage 2 embryos (Figure 12a). In advanced stage 2, *Pv_Brat*-positive cells have further increased in number, but some of them have attained a subapical position (Figure 12b). Only single cells are labeled in the NE of the antenna 2 and mandibular segments, likely corresponding to the stereotypical cells previously identified (Figure 12a). They remain identifiable even as additional cells initiate expression in more advanced stage 2 embryos (Figure 12b). The caudal papilla displays weak ubiquitous expression with marginally elevated levels in some cells that flank the midline.

In stage 3, the optic lobe and naupliar NE show strong ubiquitous expression (Figure 12c), encompassing the apical but also deeper cell layers. Next to the midline, first cells of the median protocerebrum are *Pv_Brat*-positive. Additional expression sites in the naupliar region are (1) single cells lateral to the forming stomodeum, (2) few cells in the naupliar limb buds, and (3) few cells in intersegmental positions between the limb buds (Figure 12c). In some specimens, very weak expression could be detected along the NE of the postnaupliar region as well as in a few cells lateral to the proctodeal anlage (Figure 12c).

Stage 4 retains expression in the optic lobe and naupliar NE (Figure 12d). Apart from single cells, labeling in the median protocerebral region does not cross the midline. The NE displays expression in the limb bud-bearing maxilla 1 and 2 segments. In the latter, predominantly anterior and medial neuroectodermal cells are labeled, resulting in a curved appearance of the expression domain (Figure 12d). The proctodeum is laterally flanked by a handful of *Pv_Brat*-positive cells.

FIGURE 9 *Pv_Sna1* expression in stages 2–5. Colorimetric ISH (dark blue) with Sytox nuclear counterstain (green), ventral view, stereomicroscopic (a–c) and light microscopic (d–g″) micrographs. Stars mark nonspecific surface labeling. Large black arrows mark transverse expression stripes in the developing segments. Red arrowheads mark the deutocerebral area in which a row of putative NBs develops. Asterisks highlight *Pv_Sna1*-positive cells lateral to the proctodeum. (a) Stage 2. The central stippled line indicates the posterior border of the mandibular NE. The lower stippled line marks a portion of the blastopore. Arrowheads highlight the first weakly expressing single cells in the antenna 2 and mandibular NE. Short transverse intersegmental stripes extend between the naupliar segmental anlagen (black arrows). (b) Stage 3. Single cells in and distal to the naupliar limb buds show expression (white and green arrowheads, respectively). The first cells in the forming labrum and stomodeum have initiated expression (white arrow). The small black arrows indicate single cells proximal to antenna 2 and the mandible. (c) Stage 3–4. Single cells/cell groups in the naupliar limb buds display expression (white arrowheads). A few cells in the median protocerebrum (small black arrow), in the labral anlage (white arrows), and at the midline of the naupliar/postnaupliar border (black arrowhead) are *Pv_Sna1*-positive. The stippled line outlines the forward-flexed caudal papilla. (d–g″) Stage 5. (d) The white arrow indicates strongly labeled cells in the median protocerebrum; the black arrowhead demarcates the transverse cell band at the border of the mandible and maxilla 1 segments. Single cells in the postnaupliar limb buds are *Pv_Sna1*-positive (white arrowheads). (e) Detail of the anterior head region. Cells in the proliferative region of the optic lobe (black arrow) and basally in the median protocerebrum (white arrow) show strong expression. (e′) Magnification of the deutocerebral NE. Note transverse rows of apical *Pv_Sna1*-positive cells (asterisks). The white arrow marks an apical cell with large nucleus that shows only weak expression. (f–g″) Details of the caudal papilla. Numbers indicate the position of cell columns 0–2. The right column depicts invected/engrailed immunolabeling (red). Cell d1 (white arrow) and its direct descendants d1v and the NB d1h (arrowheads) display elevated expression levels. (f–f″) Early stage 5. (g–g″) Late stage 5. The black arrowhead marks cells with elevated expression level lateral to the NE. Abbreviations: a1 and a2, antenna 1 and 2 segments; cp, caudal papilla; la, labrum; md, mandibular segment; mx1 and mx2, maxilla 1 and 2 segments; mxp1, maxilliped 1 segment; ol, optic lobe; pe1–5, pereiopod 1–5 segments

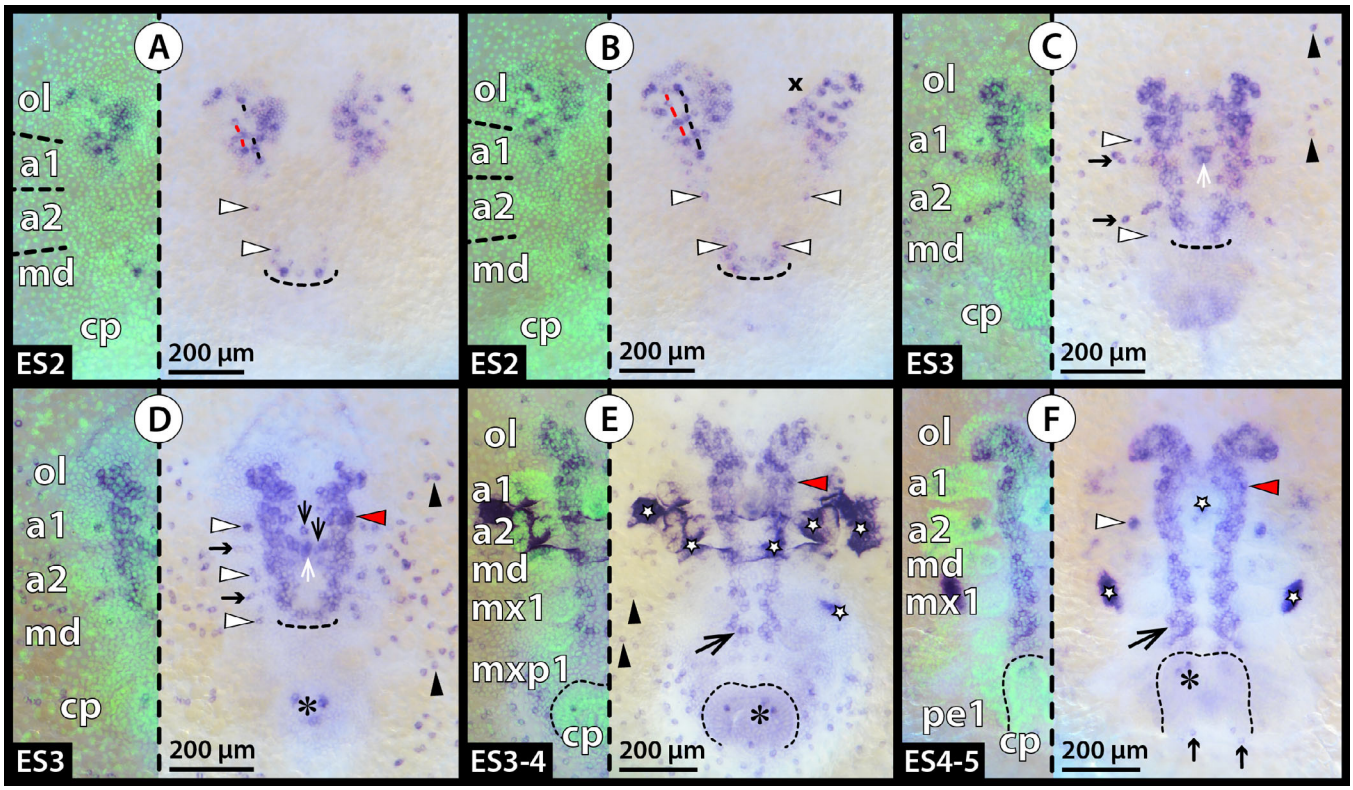

FIGURE 10 *Pv_Pros* expression in stages 2–5. Colorimetric ISH (dark blue) with Sytox nuclear counterstain (green), ventral view, stereomicroscopic micrographs. Stars (e and f) mark nonspecific surface labeling. "x" (b) marks damaged tissue. Upcurved stippled lines (a–d) mark the posterior border of the mandibular NE. Stippled lines (e and f) outline the forward-flexed caudal papilla. Asterisks (d–f) indicate *Pv_Pros*-positive cells lateral to the proctodeum. Red arrowheads (d–f) mark the deutocerebral area in which a row of putative NBs develops. Black arrowheads (c–e) point to scattered *Pv_Pros*-positive extraembryonic cells. (a and b) Stage 2. Stippled lines in the optic lobe and antenna 1 NE extend between corresponding stereotypical cells. Arrowheads indicate stereotypical cells in the antenna 2 and mandibular NE. (a) Early stage 2. Note the low number of labeled cells in the lateral optic lobe. (b) Advanced stage 2. Note the increased number (compared to panel [a]) of cells/cell groups spread out over the entire optic lobe. (c and d) Stage 3. Small black arrows mark transverse cell rows in an intersegmental position. White arrowheads highlight single cells in the naupliar limb buds. White arrows indicate the forming stomodeum. (c) Early stage 3. (d) Advanced stage 3. Medial black arrows indicate labeled cells in the labrum. Note onset of expression in the incipient caudal papilla. (e) Stage 3-4. Note onset of *Pv_Pros* expression in the NE of the anterior-most postnaupliar segments (black arrow). (f) Stage 4–5. Expression in the postnaupliar segments has increased significantly (black arrow). A spherical group of cells in the proximal portion of antenna 2 has initiated expression (white arrowhead). Abbreviations: a1 and a2, antenna 1 and 2 segments; cp, caudal papilla; md, mandibular segment; mx1, maxilla 1 segment; mxp1, maxilliped 1 segment; ol, optic lobe; pe1, pereiopod 1 segment

In stage 5, *Pv_Brat* is strongly expressed throughout the optic lobe, excluding only its distal semicircular rim (Figure 12e). The proliferative zone is *Pv_Brat* positive, but shows lower expression levels than the central cell region housing the first neurons of the lateral protocerebrum. The two hemispheres of the median protocerebrum are connected by a midline-spanning expression domain (Figure 12e). The naupliar limb buds including the gnathobasic portion of the mandible feature single cells and cell groups. In the postnaupliar region, expression extends further posteriorly, with a distinct decrease of labeled cells in the more posterior ganglionic anlagen (Figure 12e). In the telson, small groups of cells are labeled, showing a close positional correspondence to the *Pv_Elav*-positive terminal pioneer neurons (Figure 12f). In some specimens, the first NB d1h seems to show slightly elevated transcript levels, but due to low nonspecific labeling across the entire caudal papilla, we cannot exclude that this is the result of a slight overdevelopment of samples (Figure 12f).

4 | DISCUSSION

4.1 | Phylogenetic analyses of *SoxB* group, *achaete–scute* complex, and *Snail* family genes

The phylogenetic analysis of the *SoxB* group HMG box yielded results similar to previous studies of this gene class in arthropods, which likewise recovered a monophyletic clade of

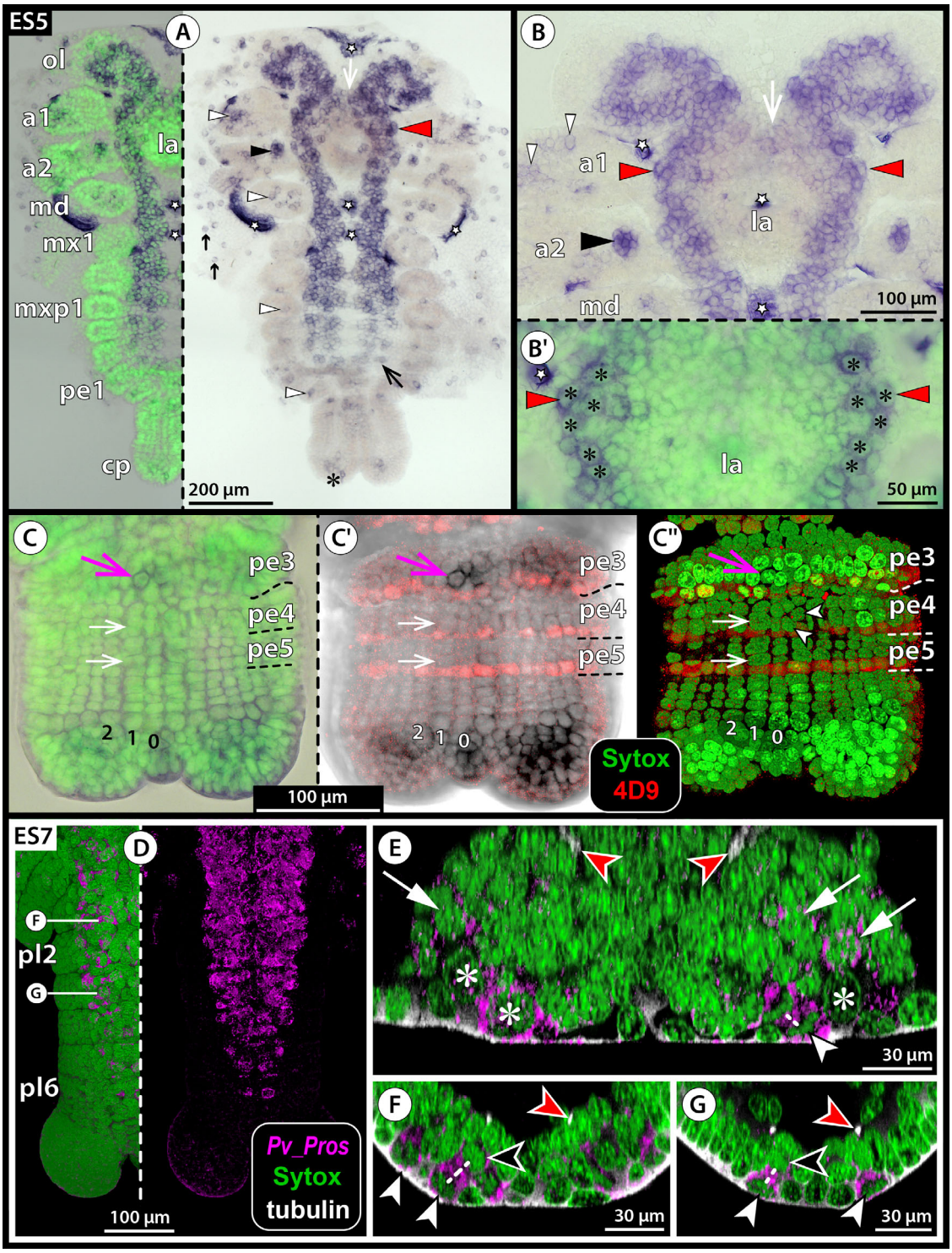

FIGURE 11 Details of *Pv_Pros* expression in stages 5 and 7. (a–c″) Stage 5. Colorimetric ISH (dark blue), Sytox nuclear counterstain (green) with additional invected/engrailed immunolabeling (red) in panels (c′) and (c″); stereomicroscopic micrographs (a–c′) and CLSM scan (c″); ventral views. Stars mark nonspecific surface labeling. Red arrowheads highlight the deutocerebral area in which a row of putative NBs develops. White arrowheads indicate *Pv_Pros*-positive cells in the limb buds. Black arrowheads point to a spherical group of cells in antenna 2. White arrows mark expression in the median protocerebrum. (a) Overview of flat preparation. An anteroposterior gradient of expression is found along the postnaupliar NE, with fewer cells being labeled in less-developed segments (large black arrow). The asterisk marks labeled cells lateral to the proctodeum, the small black arrows indicate single extraembryonic cells near the rim of the developing carapax. (b and b′) Magnification of the anterior head region. The apical layer of the NE includes presumptive NBs with slightly larger nuclei (asterisks in panel [b′]). (c–c″) Detail of the caudal papilla. Numbers indicate the position of cell columns 0–2. Cell d1 (white arrows) and its newly formed descendants d1v and d1h (white arrowheads in panel [c″]) do not display expression. Prior to the second differential division, the NB d1h has initiated transcription (magenta arrow). (d–g) Stage 7. FISH

SoxNeuro orthologs nested in a paraphyletic arrangement of *Dichaete*, *Sox21a*, and *Sox21b* members (Baudouin-Gonzalez et al., 2021; Janssen et al., 2018; Paese, Leite, et al., 2018). In support of our initial orthology assignments, the three *P. virginalis SoxB* group genes are resolved in the appropriate branch of the tree, with close relationships to the respective HMG domains of the malacostracan *M. nipponense* (Zhong et al., 2011). As of now, the *P. virginalis* draft genome does not resolve the gene arrangement of the *SoxB* group TFs at the chromosomal level. However, the available scaffolds show that *Pv_D* represents an intronless transcription unit, which is a feature shared with *Dichaete* in hexapods (McKimmie et al., 2005; Russell et al., 1996) and has similarly been indicated for *Dichaete* of the decapod crustacean *M. nipponense* (Zhong et al., 2011). In contrast, hexapod *Sox21b* genes display a multi-exon structure, including a conserved intron position within the HMG domain (Maher, 2017; McKimmie et al., 2005) that is shared by *Pv_Sox21b* and the *Sox21b* HMG domains of *M. nipponense* and of the branchiopod *Daphnia pulex* (Maher, 2017; Zhong et al., 2011). Accordingly, the genomic organization of *Pv_D* and *Pv_Sox21b* further supports our identification of these two closely related *SoxB* group genes.

The phylogenetic analyses of the *achaete–scute* complex members *ASH* and *ase*, using the bHLH domain and less well-conserved C-terminal motif, resulted in a poorly resolved topology that shows no clear separation of the two closely related gene classes. Although distinction of proneural *ASH* and NB-specific *ase* is possible within hexapods (Negre & Simpson, 2009), a previous sequence analysis covering all major arthropod taxa similarly failed to identify unequivocal non-hexapod *ase* orthologs (Ayyar et al., 2010). Nonetheless, based on a shared short five-amino-acid motif and a conserved regulatory sequences in the 5′UTR, *ase*-like genes have been suggested for branchiopod crustaceans, in spite of the fact that the accompanying phylogenetic analyses do not support orthology with hexapod *ase* (Ayyar et al., 2010). In our study, *Pv_ASH1* features a well-conserved C-terminal motif characteristic for proneural *ASH* genes and groups together with *ASH* genes of other malacostracan crustaceans. The *Pv_ASH1* expression patterns also share similarities with proneural *ASH* genes in branchiopods and hexapods. In the case of *Pv_ASH2*, the C-terminal motif is less well conserved—as is the case in many hexapod *ase* genes—but it lacks the unequivocal five-amino-acid *ase* motif. Hence, our analyses remain ambiguous and do not enable confident assignment of *Pv_ASH2* to either of the two gene classes. Future improvements in the genome assembly of *P. virginalis* may provide more insights into the gene number and genomic arrangement of the *achaete–scute* complex and thus help to clarify whether a member of this TF family in crayfish is currently still overlooked.

The phylogenetic analysis of the *Snail* TFs is in agreement with previous findings on this gene family, which indicate the occurrence of multiple independent gene duplication events during arthropod evolution (Hannibal et al., 2012; Kerner et al., 2009; Wei et al., 2016). The recovery of all three *P. virginalis Snail* TFs in a separate clade (albeit with no strong support) precludes unambiguous orthology assignment to any of the other crustacean *Snail* TFs and may point to gene duplications within decapod crustaceans, in the lineage leading to crayfish. These results mirror similar findings for the three *Snail* TFs of the amphipod *P. hawaiensis* (this study; Hannibal et al., 2012), which seem to have undergone separate duplications as well. The nested placement of *Drosophila snail* implies closer relationships between this gene (as opposed to the other two *Drosophila Snail* family members *worniu* and *escargot*) and the malacostracan *Snail* TFs.

4.2 | Further support for the homology of crustacean and hexapod NBs and their progeny

Prior to this study, the GRN underlying neurogenesis of the crustacean CNS had been studied in very few representatives and in significantly varying detail (Hannibal et al., 2012; Ungerer, Eriksson, et al., 2011; Ungerer et al., 2012; Wheeler & Skeath, 2005). Our results on *P. virginalis* complement and extend the range of genes/gene families studied and provide the first data for a crustacean on *SoxB* group TFs, *Brat* and *Elav*. Overall, the spatiotemporal expression patterns show several similarities to the NBs and their progeny in hexapods and/or branchiopod crustaceans. This includes expression of

(magenta) with Sytox nuclear counterstain (green) and tubulin immunolabeling (white in panels [e–g]), CLSM scans. (d) Ventral view of the caudal papilla; blend mode to show apical surface only (left) and maximum-intensity projection (right). Note significant decrease of labeled cells from anterior to posterior. In older neuromeres, subapical cells also show expression. (e–g) Virtual transverse sections through postnaupliar segments. Asterisks mark selected NBs in interphase. White arrowheads indicate NBs undergoing radial divisions. White arrows point to subapical cells (putative GMCs) displaying expression. Stippled lines link metaphase plates or newly forming nuclei of a NB division. Black arrowheads point to nuclei of forming GMCs. Red arrowheads highlight first longitudinal axon bundles of the growing connectives. (e) Advanced ganglionic anlage of the cheliped. Note the absence of expression in the basal cell layers. (f) Segment of the first pleopod. (g) Segment of the third pleopod. Abbreviations: a1 and a2, antenna 1 and 2 segments; cp, caudal papilla; la, labrum; md, mandibular segment; mx1, maxilla 1 segment; mxp1, maxilliped 1 segment; ol, optic lobe; pe1–5, pereiopod 1–5 segments; pl2 and pl6, pleopod 2 and 6 segments

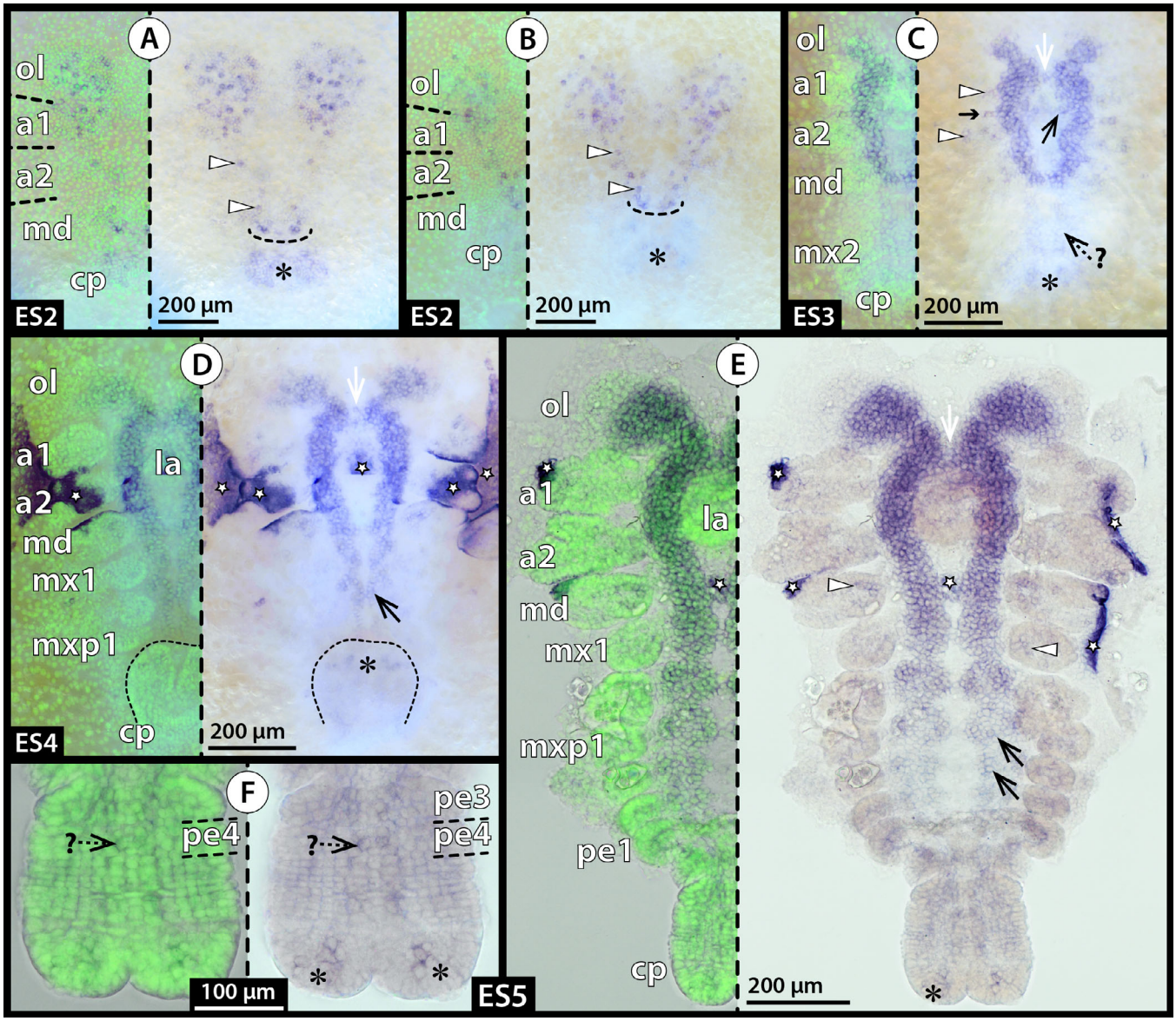

FIGURE 12 *Pv_Brat* expression in stages 2–5. Colorimetric ISH (dark blue) with Sytox nuclear counterstain (green); ventral view; stereomicroscopic (a–d) and light microscopic (e and f) micrographs. Stars mark nonspecific surface labeling. White arrows mark labeled cells in the median protocerebrum. Asterisks highlight *Pv_Brat*-positive cells lateral to the proctodeum. (a and b) White arrowheads indicate stereotypical cells in the antenna 2 and mandibular neuromere. Stippled lines mark the posterior border of the mandibular NE. (a) Early stage 2. (b) Advanced stage 2. (c) Stage 3. White arrowheads indicate cells in the naupliar limb buds. The large black arrow points to a cell near the forming labrum and stomodeum. Between the naupliar limb buds, weakly labeled transverse stripes are visible (small black arrow). The large stippled arrow indicates potential weak expression in the postnaupliar NE. (d) Stage 4. The stippled line outlines the forward-flexed caudal papilla. The postnaupliar NE features the first labeled cells (large black arrow). (e) Stage 5. White arrowheads indicate labeled cells in the limb buds. Expression extends further posteriorly along the postnaupliar NE (black arrows). (f) Detail of stage 5 caudal papilla. The stippled arrow points to putative weak expression in NB d1h. Abbreviations: a1 and a2, antenna 1 and 2 segments; cp, caudal papilla; la, labrum; md, mandibular segment; mx1 and mx2, maxilla 1 and 2 segments; mxp1, maxilliped 1 segment; ol, optic lobe; pe1–4, pereiopod 1–4 segments

1. *SoxB* group genes early on across major parts of the NE, including the NBs (Buescher et al., 2002; Crémazy et al., 2000; Janssen et al., 2018; Overton et al., 2002),
2. at least one *snail* gene in many NBs (Ashraf & Ip, 2001; Lai et al., 2012; Ungerer, Eriksson, et al., 2011; Ungerer et al., 2012),
3. *pros* in the asymmetrically dividing NBs and the newborn GMCs (Knoblich et al., 1995; Spana & Doe, 1995; Ungerer, Eriksson, et al., 2011; Vaessin et al., 1991),
4. the posttranscriptional regulator *Brat* during neural differentiation and maturation of the NB progeny (Betschinger et al., 2006; Lee et al., 2006; Reichardt et al., 2018), and

5. the RNA-binding protein *Elav* in differentiating and mature neurons (Robinow & White, 1988, 1991), making it a bona fide neuron marker.

These molecular genetic similarities between malacostracan, branchiopod, and hexapod NBs and their progeny further underpin the previously advocated cell type homologies (e.g., Ungerer & Scholtz, 2008; Ungerer, Eriksson, et al., 2011) and strengthen support for a common origin of the NB-driven neurogenesis mode of Altocrustacea (and potentially Pancrustacea in total).

4.3 | *SoxB* group TFs in the developing CNS of *P. virginalis*

As in other arthropod taxa, the three *SoxB* group TFs studied in *P. virginalis* are expressed in overlapping domains, demarcating major parts of the early embryonic NE (Buescher et al., 2002; Janssen et al., 2018; Overton et al., 2002; Paese, Leite, et al., 2018; Pioro & Stollewerk, 2006). Their broad neuroectodermal expression and the continued cell divisions in the expression domains are in line with the evolutionary conserved role of *SoxB* TFs in the GRN conferring neurogenic potential to ectodermal cells (Hartenstein & Stollewerk, 2015). Beyond this, the timing of expression may also conform with an involvement in NB formation and specification and subsequent neural differentiation, as demonstrated for *SoxNeuro* and *Dichaete* in *D. melanogaster* (Aleksic et al., 2013; Arefin et al., 2019; Buescher et al., 2002; Ferrero et al., 2014; Overton et al., 2002; Zhao & Skeath, 2002; Zhao et al., 2007). In *P. virginalis*, the specific roles of the different *SoxB* TFs during neurogenesis still need to be further elucidated with functional data.

In the naupliar region, the expression patterns in *P. virginalis* show additional parallels to hexapods, where *Pv_SoxN* is similarly expressed in the mediolaterally widest domain that extends further laterally than the *Pv_D* and *Pv_Sox21b* domains—if the latter is expressed in the NE (Janssen et al., 2018). However, in contrast to hexapods, pronounced mediolaterally staggered *SoxB* expression domains are not present in the postnaupliar NE of *P. virginalis*. Rather, the virtually identical expression domains share more similarities to *SoxB* patterns in the ventral NE of chelicerates and myriapods (Janssen et al., 2018; Pioro & Stollewerk, 2006; Paese, Leite, et al., 2018). Accordingly, the restricted lateral extension of the neuroectodermal *Pv_D* expression domain and the *Pv_SoxN*-negative midline in hexapods appear to be derived conditions that evolved within the pancrustacean lineage after the divergence of Malacostraca (i.e., in the Allotriocarida; see Schwentner et al., 2017, 2018).

At the posterior body pole of *P. virginalis*, the ETs and the earliest stages of new genealogical units lack *Pv_SoxN* expression completely. Expression sets in just prior to the first round of differential cleavages, during which the first two NBs are being formed (Alwes & Scholtz, 2006; Scholtz, 1992), and continues from that point onward in the entire NE. This tight spatiotemporal correlation strongly indicates ectodermal *Pv_SoxN* expression to be mainly—if not exclusively—embedded in the GRN underlying nervous system development. Hence, it represents a reliable neuroectodermal marker in *P. virginalis*, in agreement with other arthropod taxa (Crémazy et al., 2000; Hartenstein & Stollewerk, 2015; Janssen et al., 2018; Paese, Leite, et al., 2018).

4.4 | Involvement of *SoxB* group TFs in early segmentation of *P. virginalis*

In contrast to *Pv_SoxN*, transcription of *Pv_D* and *Pv_Sox21b* is already upregulated in the early genealogical units of *P. virginalis* prior to the onset of neurogenesis. Expression is even found in some of the posterior ETs, which are part of the well-defined subterminal growth zone of (most) malacostracan crustaceans (Fischer et al., 2010; Scholtz & Wolff, 2013). This situation corresponds to other arthropod taxa that are characterized by a sequential segment addition at the posterior body pole, where *Dichaete* and—if studied—also *Sox21b* are expressed in the posterior segment addition zone (SAZ) (Baudouin-Gonzalez et al., 2021; Clark & Peel, 2018; Janssen et al., 2018; Paese, Leite, et al., 2018; Paese, Schoenauer, et al., 2018). In hexapods, *Dichaete* has been shown experimentally to play an important role in the regulation of segmentation (Clark & Peel, 2018; Russell et al., 1996). By contrast, recent studies in a spider revealed a similar function for one of its *Sox21b* genes instead of *Dichaete*, which was subsequently proposed to represent the ancestral condition for the entire arachnid lineage (Baudouin-Gonzalez et al., 2021; Paese, Schoenauer, et al., 2018). In *P. virginalis*, *Pv_D* expression shares more similarities with hexapods, as it features transient transverse stripes that extend laterally to the NE in some of the early segmental anlagen. An in-depth expression pattern analysis over earlier and later embryonic stages is pending, but our first observations may point to a role of *Pv_D* (instead of *Pv_Sox21b*) during segmentation in *P. virginalis*, which may thus qualify as the plesiomorphic state of Pancrustacea.

At the posterior pole of *P. virginalis*, we found that expression of *Pv_D* and *Pv_Sox21b* includes the ETs of cell columns 3 and 4, but does not reach further dorsally along the ET ring. This suggests that both genes also play a role in the dorsoventral patterning of the early cell material of the genealogical units. Moreover, with ongoing development, all three *SoxB* group TFs studied become increasingly upregulated in telson cells posterior to the ETs, that is, in the terminal region that does not contribute cell material to segment formation. Except for part of the *Pv_D* expression, which is at least transiently upregulated in the forming proctodeal anlage as in

Drosophila (Sánchez-Soriano & Russell, 2000), it remains unclear to which developmental processes the overlapping telsonic *SoxB* expression domains in *P. virginalis* relate. High-resolution *SoxB* TF expression studies in non-pancrustacean arthropod taxa would be desirable to unravel whether their reported dynamic patterns in the SAZ can be likewise subdivided into subterminal cell areas involved in segment formation and more terminal telson domains.

4.5 | Expression of *achaete–scute* complex and *Snail* TFs in the ventral NE

During arthropod neurogenesis, *ASH* TFs have been shown to serve a proneural function, that is, they are part of the GRN that confers ectodermal cells neurogenic potential (Hartenstein & Stollewerk, 2015; Stollewerk, 2016). In the ventral NE of hexapods, *ASH* TFs are expressed early on in a spatiotemporally invariant pattern of small cell groups, the so-called proneural clusters (Cabrera et al., 1987; Skeath & Thor, 2003; Wheeler et al., 2003). In each of the proneural clusters, a future NB is selected via *Notch* signaling-mediated lateral inhibition and immigrates into subapical position prior to the onset of its asymmetrical divisions. In similar fashion, spatiotemporally invariant *ASH*-expressing domains characterize early neurogenesis in chelicerates and myriapods (Dove & Stollewerk, 2003; Kadner & Stollewerk, 2004; Stollewerk et al., 2001, 2003). However, at the cellular level, no stem cell-like dividing NBs are selected in these domains but groups of predominantly postmitotic neural precursors that emigrate from the NE and for the most part undergo neural differentiation directly. In contrast to emigrating NBs or neural precursors, all crustacean taxa hitherto studied feature NBs that remain in the apical NE while budding off neural progeny into the embryo via radial divisions (Dohle, 1976; Hein & Scholtz, 2018; Scholtz, 1990, 1992; Ungerer & Scholtz, 2008; Ungerer, Eriksson, et al., 2011). In branchiopod crustaceans, the NBs also express an *ASH* TF (Ungerer, Eriksson, et al., 2011; Wheeler & Skeath, 2005) but are not selected from proneural clusters. In the water flea *Daphnia magna*, NBs are formed next to each other in the apical NE, and NB-specific upregulation of a *Snail* TF predates the first expression of *ASH*. This could indicate that *Snail* acts as neural fate determinant for branchiopod NBs, whereas *ASH* is only involved in maintenance of the already formed NBs in the surrounding epidermal environment and the regulation of further genes of the neurogenic GRN (Ungerer, Eriksson, et al., 2011). One of the latter could be the second *achaete–scute* complex gene of branchiopods, which is subsequently expressed in the NBs and displays some sequence similarity to *ase* of hexapods (Ayyar et al., 2010; Ungerer, Eriksson, et al., 2011; Ungerer et al., 2012; Wheeler & Skeath, 2005). In line with the persistent NB-specific expression of hexapod *ase* (Biffar & Stollewerk, 2014; Jarman et al., 1993; Wheeler et al., 2003), this *ase*-like gene of branchiopods represents a reliable NB marker (Ungerer, Eriksson, et al., 2011; Ungerer et al., 2012; Wheeler & Skeath, 2005).

Our results on the *achaete–scute* complex and *Snail* TFs in the malacostracan *P. virginalis* deviate in part from the findings in branchiopod crustaceans. *Pv_Sna1* displays distinct ectodermal expression in cell columns 1 and 2, already prior to the formation of the first NBs and the onset of *Pv_ASH1* expression, which is in line with the potential proneural function suggested for branchiopod *Snail*. However, *Pv_ASH1* is transiently upregulated not only in the newly formed first NB d1h but for a shorter time span also in its nonneural sister cell d1v. Only after this period of strong *Pv_ASH1* expression, NB d1h starts its characteristic radially directed neurogenic divisions (see Scholtz, 1992 for crayfish cell lineage). This location and timing of *Pv_ASH1* upregulation is to some extent reminiscent of the *achaete–scute* complex expression in hexapod proneural clusters, in which only the nascent NB retains high ASH transcript levels (Skeath & Carroll, 1992; Skeath & Thor, 2003). Accordingly, this may indicate *Pv_ASH1* to represent another neural determinant in *P. virginalis*, acting in concert with *Pv_Sna1* during NB formation. Although differing from the current model of NB formation in branchiopods (Ungerer, Eriksson, et al., 2011), the suggested interplay of different proneural genes during malacostracan NB formation shows correspondences to hexapods. In *Drosophila*, a proneural role has been recently revealed for several non-*achaete–scute* complex genes (Arefin et al., 2019), including not only the *Snail* family member *worniu* but also *SoxNeuro*, which is similarly co-expressed in the NE of *P. virginalis* during NB formation.

Notably, the ventral NE of *P. virginalis* displays no significant *Pv_ASH2* transcription in any of the embryonic stages studied; its distinct upregulation is instead exclusively restricted to the naupliar region. This contrasts to the *ase* expression in hexapods (Biffar & Stollewerk, 2014; Jarman et al., 1993; Wheeler et al., 2003) and the *ase*-like expression of the second *achaete–scute* complex TF identified in branchiopods (Ungerer, Eriksson, et al., 2011; Wheeler & Skeath, 2005). Based on the lack of any additional *achaete–scute* complex candidate sequences in the developmental transcriptomes and draft genome of *P. virginalis*, we therefore cautiously conclude that the GRN controlling NB maintenance in the ventral NE of crayfish does not involve an *Ase*-like TF.

4.6 | Initial neurogenesis in the naupliar region driven by neural progenitors of non-NB nature?

Compared to other arthropod groups, our understanding of the earliest cellular processes of malacostracan brain

development is still in its infancy. Several traditional histological studies contain cursory observations on cell patterns in the naupliar region (e.g., Reichenbach, 1886; Shiino, 1942, 1950; Weygoldt, 1961; Zehnder, 1934), whereas more recent investigations have mainly dealt with brain axogenesis, that is, focused on the differentiation of already internalized postmitotic neurons, but not their origin (Biffis, 2017; Fischer & Scholtz, 2010; Harzsch et al., 1997; Ungerer, Geppert, et al., 2011; Vilpoux et al., 2006).

Similar to the ventral NE, spatiotemporally invariant emigration of cells committed to the neural pathway is a common motif of early brain neurogenesis in non-crustacean arthropods (Brenneis, 2013; Doeffinger et al., 2010; Urbach et al., 2003; Urbach & Technau, 2003; Younossi-Hartenstein et al., 1996). Also in *P. virginalis*, cell emigration from the naupliar NE leads to internalization of the first cells during stage 2, prior to the formation of the first brain NBs in stage 3. The emigrating cells are *Pv_SoxN*-positive and show no spatial correlation to divisions in the apical NE. Further, the detection of single internally displaced cells in some of the invariant *Pv_ASH1* expression sites suggests that only a few cells are selected from the apical *Pv_ASH1* domains, in correspondence to proneural clusters in the developing hexapod brain (e.g., Urbach et al., 2003). Based on pattern comparison across stage 2 embryos, several of these *Pv_ASH1*-expressing cells appear to also show upregulation of *Pv_ASH2*, which is reminiscent of a NB-specific expression of *ase* in hexapods (Biffar & Stollewerk, 2014; Brand et al., 1993; Jarman et al., 1993; Wheeler et al., 2003) and *ase*-like/*ASH2* of branchiopods (Ungerer, Eriksson, et al., 2011; Wheeler & Skeath, 2005). Future double labeling of both *achaete–scute* complex genes in *P. virginalis* will be needed to elucidate the timing of this likely co-expression in more detail.

Interestingly, the differences in *Pv_ASH1* and *Pv_ASH2* expression between the naupliar and postnaupliar regions correlate with the deviating processes underlying the formation of both regions in malacostracan crustaceans. While the naupliar ectoderm is formed via cell condensation and (seemingly) unordered proliferation into a germ disc as in many other arthropods, the postnaupliar ectoderm arises by the unique stereotypical division cascade of the ET progeny. As this mode of postnaupliar segment formation via an invariant cell lineage is an apomorphic character of malacostracan crustaceans (Fischer et al., 2010; Scholtz & Wolff, 2013), the concomitant lack of expression of a second, NB-specific *achaete-scute* complex TF during early neurogenesis may be a derived malacostracan character as well.

Further comparison of expression patterns in the naupliar region of stage 2 shows that many of the *Pv_ASH1*- and *Pv_ASH2*-positive cells seem to co-express *Pv_Pros*, *Pv_Sna1*, and *Pv_Brat*, which enables their identification as the first cells committed to the neural pathway and confirms histology-based interpretations on other malacostracans (Shiino, 1942, 1950; Weygoldt, 1961). Notably, however, the concomitant expression of *Pv_Pros* and *Pv_Brat* speaks against their NB nature but rather points to directly differentiating neural precursors. Both genes are known to be key for inhibition of self-renewal and promotion of neural differentiation in the progeny of hexapod NBs (Bello et al., 2006; Betschinger et al., 2006; Li & Vaessin, 2000; Reichardt et al., 2018; Spana & Doe, 1995; Vaessin et al., 1991). Further support for direct neural differentiation comes from a description of brain axogenesis in *P. virginalis*, reporting first axonal projections in the protocerebral and deutocerebral neuromeres already in early stage 3 (Biffis, 2017), at a time when the first enlarged NBs only start to appear in the apical NE. Based on these findings, we propose that the initial phase of brain neurogenesis in crayfish and other malacostracans is not driven by stem cell-like dividing NBs.

Notably, sequential formation of different neural precursor/progenitor types during CNS development is also known for other arthropod groups, such as the chelicerate Pycnogonida (sea spiders). Here, neural progenitors with stem cell-like characteristics are formed only after an initial emigration of postmitotic neural precursors from the head lobe and ventral NE at invariant sites (Brenneis, 2013; Brenneis et al., 2013). Likewise, hexapod brain neurogenesis is also not completely reliant on NBs (e.g., Boyan et al., 2003; Boyan & Williams, 2008; de Velasco et al., 2007). For instance, the preoral protocerebral commissure in the desert locust *Schistocerca gregaria* is established by a set of pioneer neurons that differentiate directly from postmitotic neural precursors that emigrate in the anteromedian pars intercerebralis (Boyan et al., 2003; Boyan & Williams, 2008; Ludwig et al., 1999). Interestingly, a similar set of protocerebral pioneer neurons has also been discovered during axogenesis in the malacostracan crustacean *Cryptorchestia cavimana* (see Ungerer, Geppert, et al., 2011). Although cell lineage studies for these pioneer neurons are pending in malacostracans, their derivation from emigrating postmitotic cells is rendered plausible given our present observations on the first neural precursors in the crayfish brain. This potentially shared mode of protocerebral commissure pioneering in hexapods and crustaceans also shows correspondences to brain development in centipedes (Hunnekuhl & Akam, 2014). Hence, the development of the very first protocerebral commissural neurons from cells that are directly specified in the apical NE may represent an evolutionarily conserved character for Mandibulata.

4.7 | Perspective: Molecular genetic characterization of adult neurogenesis in Malacostraca

The brain of several malacostracan taxa has been shown to possess centers of life-long neurogenesis in the

protocerebrum (e.g., Schmidt, 1997; Schmidt & Harzsch, 1999; Sullivan & Beltz, 2005) and deutocerebrum (e.g., Sandeman et al., 2011; Wittfoth & Harzsch, 2018). Especially in decapods, the adult deutocerebral proliferative system (DPS; sensu Wittfoth & Harzsch, 2018), which is involved in the production of olfactory local interneurons and projection neurons, has been intensely studied (Chaves da Silva et al., 2012; Schmidt, 2001, 2007; Sullivan & Beltz, 2005; Sullivan, Benton, et al., 2007; Sullivan, Sandeman, et al., 2007). One of the contested issues pertains to the nature of the neural founder cells in the decapod DPS. In spiny lobsters as well as in dendrobranchiate and caridean shrimps, a NB has been proposed to drive adult neurogenesis (Schmidt, 2007; Schmidt & Derby, 2011; Wittfoth & Harzsch, 2018). By contrast, the DPS in crayfish does not seem to rely on NBs, featuring instead neural progenitors with limited proliferation potential that are replenished over time by hemocytes from the innate immune system (Benton et al., 2011, 2014; Brenneis & Beltz, 2020). To this day, however, studies on the GRN of these adult neurogenic processes and a molecular genetic characterization of the cell types involved are pending. In *P. virginalis*, DPS formation begins during late embryonic development in a deutocerebral region that is characterized by a transverse proliferative cell band including NBs, which in part still co-exist with the incipient DPS (Sintoni et al., 2012). In the present study, the deutocerebral NBs in the area of prospective DPS formation have been shown to express several of the target genes, including the three *SoxB* group TFs, *Pv_Sna1*, the neural differentiation factor *Pv_Pros*, as well as the *achaete–scute* complex member *Pv_ASH2*. Hence, this set of genes may prove useful for the molecular investigation of early DPS development among the deutocerebral NBs. Beyond this, our suite of first target genes also promises to be a suitable starting point for the molecular genetic characterization of subregions and different cell types in the fully formed adult DPS itself.

ACKNOWLEDGMENTS

Pat Carey and Valerie LePage took care of the berried *P. virginalis* and *P. clarkii* females used in the studies. Yui Suzuki and Prashant Sharma gave valuable advice on the optimization of in situ hybridization protocols. Frank Lyko and Julian Gutekunst are thanked for granting access to the draft genome of *P. virginalis* prior to its publication. Anastasios Pavlopoulos provided a developmental transcriptome of *P. hawaiensis* for the identification of *SoxB* group and *achaete–scute* complex sequences. Gerhard Scholtz and Steffen Harzsch are thanked for constructive comments and for providing elusive literature. GB received funding from the Deutsche Forschungsgemeinschaft (DFG; grant nos. BR5039/1-1, BR5039/3-1). *Procambarus clarkii* transcriptome work was supported by internal funds from the Museum of Comparative Zoology (Harvard University). The project was supported by a National Science Foundation grant to BSB (NSF-IOS-1656103).

Open access funding enabled and organized by Projekt DEAL.

CONFLICTS OF INTEREST

The authors declare no conflicts of interest.

DATA AVAILABILITY STATEMENT

All target gene sequences have been deposited in GenBank (File S5). The remaining data that support the findings of this study are available from the corresponding authors upon reasonable request.

ORCID

Georg Brenneis https://orcid.org/0000-0003-1202-1899

REFERENCES

Aleksic, J., Ferrero, E., Fischer, B., Shen, S. P., & Russell, S. (2013). The role of *Dichaete* in transcriptional regulation during *Drosophila* embryonic development. *BMC Genomics*, *14*, 861. https://doi.org/10.1186/1471-2164-14-861

Alwes, F., & Scholtz, G. (2006). Stages and other aspects of the embryology of the parthenogenetic Marmorkrebs (Decapoda, Reptantia, Astacida). *Development, Genes and Evolution*, *216*, 169–184. https://doi.org/10.1007/s00427-005-0041-8

Arefin, B., Parvin, F., Bahrampour, S., Stadler, C. B., & Thor, S. (2019). *Drosophila* neuroblast selection is gated by Notch, Snail, SoxB, and EMT gene interplay. *Cell Reports*, *29*(11), 3636–3651.e3. https://doi.org/10.1016/j.celrep.2019.11.038

Ashraf, S. I., & Ip, Y. T. (2001). The Snail protein family regulates neuroblast expression of *inscuteable* and *string*, genes involved in asymmetry and cell division in *Drosophila*. *Development*, *128*, 4757–4767. https://doi.org/10.1242/dev.128.23.4757

Ashraf, S. I., Hu, X., Roote, J., & Ip, Y. T. (1999). The mesoderm determinant Snail collaborates with related zinc-finger proteins to control *Drosophila* neurogenesis. *The EMBO Journal*, *18*, 6426–6438. https://doi.org/10.1093/emboj/18.22.6426

Ayyar, S., Negre, B., Simpson, P., & Stollewerk, A. (2010). An arthropod *cis*-regulatory element functioning in sensory organ precursor development dates back to the Cambrian. *BMC Biology*, *8*, 127. https://doi.org/10.1186/1741-7007-8-127

Baudouin-Gonzalez, L., Schoenauer, A., Harper, A., Blakeley, G., Seiter, M., Arif, S., Sumner-Rooney, L., Russell, S., Sharma, P. P., & McGregor, A. P. (2021). The evolution of Sox gene repertoires and regulation of segmentation in arachnids. *Molecular Biology and Evolution*, *38*, 3153–3169, https://doi.org/10.1093/molbev/msab088

Bello, B., Reichert, H., & Hirth, F. (2006). The *brain tumor* gene negatively regulates neural progenitor cell proliferation in the larval central brain of *Drosophila*. *Development*, *133*, 2639–2648. https://doi.org/10.1242/dev.02429

Benton, J. L., Kery, R., Li, J., Noonin, C., Söderhäll, I., & Beltz, B. S. (2014). Cells form the immune system generate adult-born neurons in crayfish. *Developmental Cell*, *30*, 322–333. https://doi.org/10.1016/j.devcel.2014.06.016

Benton, J. L., Zhang, Y., Kirkhart, C. R., Sandeman, D. C., & Beltz, B. S. (2011). Primary neuronal precursors in adult crayfish brain: Replenishment from a non-neuronal source. *BMC Neuroscience*, *12*, 53. https://doi.org/10.1186/1471-2202-12-53

Betschinger, J., Mechtler, K., & Knoblich, J. A. (2006). Asymmetric segregation of the tumor suppressor *brat* regulates self-renewal in *Drosophila* neural stem cells. *Cell*, *124*, 1241–1253. https://doi.org/10.1016/j.cell.2006.01.038

Biffar, L., & Stollewerk, A. (2014). Conservation and evolutionary modifications of neuroblast expression patterns in insects. *Developmental Biology*, *388*, 103–116. https://doi.org/10.1016/j.ydbio.2014.01.028

Biffis, C. (2017). *Comparative studies in the development of the nervous system in malacostracan crustaceans* (Ph.D. thesis). Humboldt-Universität zu Berlin.

Boyan, G., & Williams, J. L. D. (2008). Evidence that the primary brain commissure is pioneered by neurons with a peripheral-like ontogeny in the grasshopper *Schistocerca gregaria*. *Arthropod Structure and Development*, *37*, 186–198. https://doi.org/10.1016/j.asd.2007.10.002

Boyan, G. S., Reichert, H., & Hirth, F. (2003). Commissure formation in the embryonic insect brain. *Arthropod Structure and Development*, *32*, 61–77. https://doi.org/10.1016/S1467-8039(03)00037-9

Brand, M., Jarman, A. P., Jan, L. Y., & Jan, Y. N. (1993). *Asense* is a *Drosophila* neural precursor gene and is capable of initiating sense organ formation. *Development*, *119*, 1–17. https://doi.org/10.1242/dev.119.1.1

Brenneis, G. (2013). *On the embryonic and post-embryonic development of Pseudopallene sp. (Arthropoda, Pycnogonida) with special focus on neurogenesis and nervous system differentiation* (Ph.D. thesis). Humboldt Universität zu Berlin.

Brenneis, G., & Beltz, B. S. (2020). Adult neurogenesis in crayfish: Origin, expansion, and migration of neural progenitor lineages in a pseudostratified neuroepithelium. *The Journal of Comparative Neurology*, *528*, 1459–1485. https://doi.org/10.1002/cne.24820

Brenneis, G., Stollewerk, A., & Scholtz, G. (2013). Embryonic neurogenesis in *Pseudopallene* sp. (Arthropoda, Pycnogonida) includes two subsequent phases with similarities to different arthropod groups. *EvoDevo*, *4*, 32. https://doi.org/10.1186/2041-9139-4-32

Buescher, M., Hing, F. S., & Chia, W. (2002). Formation of neuroblasts in the embryonic central nervous system of *Drosophila melanogaster* is controlled by *SoxNeuro*. *Development*, *129*, 4193–4203. https://doi.org/10.1242/dev.129.18.4193

Cabrera, C. V., Martinez-Arias, A., & Bate, M. (1987). The expression of three members of the *achaete-scute* gene complex correlates with neuroblast segregation in *Drosophila*. *Cell*, *50*, 425–433. https://doi.org/10.1016/0092-8674(87)90496-X

Cai, Y., Chia, W., & Yang, X. (2001). A family of Snail-related zinc finger proteins regulates two distinct and parallel mechanisms that mediate *Drosophila* neuroblast asymmetric divisions. *The EMBO Journal*, *20*, 1704–1714. https://doi.org/10.1093/emboj/20.7.1704

Campos, A. R., Grossman, D., & White, K. (1985). Mutant alleles at the locus *elav* in *Drosophila melanogaster* lead to nervous system defects. A developmental-genetic analysis. *Journal of Neurogenetics*, *2*, 197–218. https://doi.org/10.3109/01677068509100150

Chaves da Silva, P. G., Benton, J. L., Beltz, B. S., & Allodi, S. (2012). Adult neurogenesis: Ultrastructure of a neurogenic niche and neurovascular relationships. *PLoS ONE*, *7*, e39267. https://doi.org/10.1371/journal.pone.0039267

Chien, H., Tadesse, T., Liu, H., Schmidt, M., Walthall, W. W., Tai, P. C., & Derby, C. D. (2009). Molecular cloning and characterization of homologs of *achaete-scute* and *hairy-enhancer of split* in the olfactory organ of the spiny lobster *Panulirus argus*. *Journal of Molecular Neuroscience*, *39*, 294–307. https://doi.org/10.1007/s12031-009-9195-6

Choksi, S. P., Southall, T. D., Bossing, T., Edoff, K., de Wit, E., Fischer, B. E., Steensel, B., Micklem, G., & Brand, A. H. (2006). *Prospero* acts as a binary switch between self-renewal and differentiation in *Drosophila* neural stem cells. *Developmental Cell*, *11*, 775–789. https://doi.org/10.1016/j.devcel.2006.09.015

Chu-LaGraff, Q., Wright, D. M., McNeil, L. K., & Doe, C. Q. (1991). The *prospero* gene encodes a divergent homeodomain protein that controls neuronal identity in *Drosophila*. *Development Supplement*, *2*, 79–85.

Clark, E., & Peel, A. D. (2018). Evidence for the temporal regulation of insect segmentation by a conserved sequence of transcription factors. *Development*, *145*(10), dev155580. https://doi.org/10.1242/dev.155580

Crémazy, F., Berta, P., & Girard, F. (2000). *Sox Neuro*, a new *Drosophila* Sox gene expressed in the developing central nervous system. *Mechanisms of Development*, *93*, 215–219. https://doi.org/10.1016/S0925-4773(00)00268-9

Crews, S. T. (2019). *Drosophila* embryonic CNS development: Neurogenesis, gliogenesis, cell fate, and differentiation. *Genetics*, *213*, 1111–1144. https://doi.org/10.1534/genetics.119.300974

de Velasco, B., Erclik, T., Shy, D., Sclafani, J., Lipshitz, H., McInnes, R., & Hartenstein, V. (2007). Specification and development of the pars intercerebralis and pars lateralis, neuroendocrine command centers in the *Drosophila* brain. *Developmental Biology*, *302*, 309–323. https://doi.org/10.1016/j.ydbio.2006.09.035

Doe, C. Q., Chu-LaGraff, Q., Wright, D. M., & Scott, M. P. (1991). The *prospero* gene specifies cell fates in the *Drosophila* central nervous system. *Cell*, *65*, 451–464. https://doi.org/10.1016/0092-8674(91)90463-9

Doeffinger, C., Hartenstein, V., & Stollewerk, A. (2010). Compartmentalisation of the precheliceral neuroectoderm in the spider *Cupiennius salei*: Development of the arcuate body, the optic ganglia and the mushroom body. *The Journal of Comparative Neurology*, *518*, 2612–2632.

Dohle, W. (1976). Die Bildung und Differenzierung des postnauplialen Keimstreifs von *Diastylis rathkei* (Crustacea, Cumacea). II. Die Differenzierung und Musterbildung des Ektoderms. *Zoomorphologie*, *84*, 235–277. https://doi.org/10.1007/BF01578696

Dove, H., & Stollewerk, A. (2003). Comparative analysis of neurogenesis in the myriapod *Glomeris marginata* (Diplopoda) suggests more similarities to chelicerates than to insects. *Development*, *130*, 2161–2171. https://doi.org/10.1242/dev.00442

Duman-Scheel, M., & Patel, N. H. (1999). Analysis of molecular marker expression reveals neuronal homology in distantly related arthropods. *Development*, *126*, 2327–2334. https://doi.org/10.1242/dev.126.11.2327

Fabritius-Vilpoux, K., Bisch-Knaden, S., & Harzsch, S. (2008). Engrailed-like immunoreactivity in the embryonic ventral nerve cord of the Marbled Crayfish (Marmorkrebs). *Invertebrate Neuroscience*, *8*, 177–197. https://doi.org/10.1007/s10158-008-0081-7

Ferrero, E., Fischer, B., & Russell, S. (2014). *SoxNeuro* orchestrates central nervous system specification and differentiation in *Drosophila* and is only partially redundant with *Dichaete*. *Genome Biology*, *15*, R74. https://doi.org/10.1186/gb-2014-15-5-r74

Fischer, A. H. L., & Scholtz, G. (2010). Axogenesis in the stomatopod crustacean *Gonodactylaceus falcatus* (Malacostraca). *Invertebrate Biology*, *129*, 59–76. https://doi.org/10.1111/j.1744-7410.2010.00192.x

Fischer, A. H., Pabst, T., & Scholtz, G. (2010). Germ band differentiation in the stomatopod *Gonodactylaceus falcatus* and the origin of the stereotyped cell division pattern in Malacostraca (Crustacea). *Arthropod Structure and Development*, *39*, 411–422. https://doi.org/10.1016/j.asd.2010.05.006

Gutekunst, J., Andriantsoa, R., Falckenhayn, C., Hanna, K., Stein, W., Rasamy, J., & Lyko, F. (2018). Clonal genome evolution and rapid invasive spread of the marbled crayfish. *Nature Ecology and Evolution*, *222*, 139–151.

Hannibal, R. L., Price, A. L., Parchem, R. J., & Patel, N. H. (2012). Analysis of *snail* genes in the crustacean *Parhyale hawaiensis*: Insight into *snail* gene family evolution. *Development, Genes and Evolution*, *222*, 139–151. https://doi.org/10.1007/s00427-012-0396-6

Hartenstein, V., & Stollewerk, A. (2015). The evolution of early neurogenesis. *Developmental Cell*, *32*, 390–407. https://doi.org/10.1016/j.devcel.2015.02.004

Harzsch, S., Anger, K., & Dawirs, R. R. (1997). Immunocytochemical detection of acetylated α-tubulin and *Drosophila* synapsin in the embryonic crustacean nervous system. *International Journal of Developmental Biology*, *41*, 477–484.

Harzsch, S., Krieger, J., & Faulkes, Z. (2015). Crustacea": Decapoda - Astacida. In A. Wanninger (Ed.), Evolutionary developmental biology of invertebrates 4: Ecdysozoa II: "Crustacea" (pp. 101–151). Springer-Verlag.

Hein, H., & Scholtz, G. (2018). Larval neurogenesis in the copepod *Tigriopus californicus* (Tetraconata, Multicrustacea). *Development, Genes and Evolution*, *228*, 119–129. https://doi.org/10.1007/s00427-018-0610-2

Homen, C., & Knoblich, J. A. (2012). *Drosophila* neuroblasts: A model for stem cell biology. *Development*, *139*, 4297–4310. https://doi.org/10.1242/dev.080515

Hunnekuhl, V. S., & Akam, M. (2014). An anterior medial cell population with an apical-organ-like transcriptional profile that pioneers the central nervous system in the centipede *Strigamia maritima*. *Developmental Biology*, *396*, 136–149. https://doi.org/10.1016/j.ydbio.2014.09.020

Janssen, R., Andersson, E., Betnér, E., Bijl, S., Fowler, W., Höök, L., Leyhr, J., Mannelqvist, A., Panara, V., Smith, K., & Tiemann, S. (2018). Embryonic expression patterns and phylogenetic analysis of panarthropod sox genes: Insight into nervous system development, segmentation and gonadogenesis. *BMC Evolutionary Biology*, *18*, 88. https://doi.org/10.1186/s12862-018-1196-z

Jarman, A. P., Brand, M., Jan, L. Y., & Jan, Y. N. (1993). The regulation and function of the helix-loop-helix gene, *asense*, in *Drosophila* neural precursors. *Development*, *119*, 19–29. https://doi.org/10.1242/dev.119.1.19

Jiménez, F., & Campos-Ortega, J. A. (1990). Defective neuroblast commitment in mutants of the *achaete-scute* complex and adjacent genes of *D. melanogaster*. *Neuron*, *5*, 81–89. https://doi.org/10.1016/0896-6273(90)90036-F

Kadner, D., & Stollewerk, A. (2004). Neurogenesis in the chilopod *Lithobius forficatus* suggests more similarities to chelicerates than to insects. *Development, Genes and Evolution*, *214*, 367–379. https://doi.org/10.1007/s00427-004-0419-z

Kang, K. H., & Reichert, H. (2015). Control of neural stem cell self-renewal and differentiation in *Drosophila*. *Cell and Tissue Research*, *359*, 33–45. https://doi.org/10.1007/s00441-014-1914-9

Katoh, K., & Standley, D. (2013). MAFFT multiple sequence alignment software version 7: Improvements in performance and usability. *Molecular Biology and Evolution*, *30*, 772–780. https://doi.org/10.1093/molbev/mst010

Kerner, P., Hung, J., Béhague, J., Le Gouar, M., Balavoine, G., & Vervoort, M. (2009). Insights into the evolution of the *snail* superfamily from metazoan wide molecular phylogenies and expression data in annelids. *BMC Evolutionary Biology*, *9*, 94. https://doi.org/10.1186/1471-2148-9-94

Knoblich, J. A., Jan, L. Y., & Jan, Y. N. (1995). Asymmetric segregation of Numb and Prospero during cell division. *Nature*, *377*, 624–627. https://doi.org/10.1038/377624a0

Koushika, S. P., Lisbin, M. J., & White, K. (1996). ELAV, a *Drosophila* neuron-specific protein, mediates the generation of an alternatively spliced neural protein isoform. *Current Biology*, *6*, 1634–1641. https://doi.org/10.1016/S0960-9822(02)70787-2

Kumar, S., Stecher, G., Li, M., Knyaz, C., & Tamura, K. (2018). MEGA X: Molecular Evolutionary Genetics Analysis across computing platforms. *Molecular Biology and Evolution*, *35*, 1547–1549. https://doi.org/10.1093/molbev/msy096

Lai, S. - L., Miller, M. R., Robinson, K. J., & Doe, C. Q. (2012). The *snail* family member *worniu* is continuously required in neuroblasts to prevent *elav*-induced premature differentiation. *Developmental Cell*, *23*, 849–857. https://doi.org/10.1016/j.devcel.2012.09.007

Lee, C. Y., Wilkinson, B. D., Siegrist, S. E., Wharton, R. P., & Doe, C. Q. (2006). *Brat* is a *Miranda* cargo protein that promotes neuronal differentiation and inhibits neuroblast self-renewal. *Developmental Cell*, *10*, 441–449. https://doi.org/10.1016/j.devcel.2006.01.017

Lee, S., Wei, L., Zhang, B., Goering, R., Majumdar, S., Wen, J., Taliaferro, J. M., & Lai, E. C. (2021). ELAV/Hu RNA binding proteins determine multiple programs of neural alternative splicing. *PLoS Genetics*, *17*(4), e1009439. https://doi.org/10.1371/journal.pgen.1009439

Li, L., & Vaessin, H. (2000). Pan-neural Prospero terminates cell proliferation during *Drosophila* neurogenesis. *Genes and Development*, *14*, 147–151.

Liu, X., Shen, J., Xie, L., Wei, Z., Wong, C., Li, Y., Zheng, X., Li, P., & Song, Y. (2020). Mitotic implantation of the transcription factor Prospero via phase separation drives terminal neuronal differentiation. *Developmental Cell*, *52*, 277–293.e8. https://doi.org/10.1016/j.devcel.2019.11.019

Loedige, I., Jakob, L., Treiber, T., Ray, D., Stotz, M., Treiber, N., Hennig, J., Cook, K. B., Morris, Q., Hughes, T. R., Engelmann, J. C., Krah, M. P., & Meister, G. (2015). The crystal structure of the NHL domain in complex with RNA reveals the molecular basis of *Drosophila* Brain-Tumor-mediated gene regulation. *Cell Reports*, *13*, 1206–1220. https://doi.org/10.1016/j.celrep.2015.09.068

Ludwig, P., Williams, J. L. D., Lodde, E., Reichert, H., & Boyan, G. S. (1999). Neurogenesis in the median domain of the embryonic brain of the grasshopper *Schistocerca gregaria*. *The Journal of Comparative Neurology*, *414*, 379–390. https://doi.org/10.1002/(SICI)1096-9861(19991122)414:3%3c379::AID-CNE7%3e3.0.CO;2-5

Lyko, F. (2017). The marbled crayfish (Decapoda: Cambaridae) represents an independent new species. *Zootaxa*, *4363*, 544–552. https://doi.org/10.11646/zootaxa.4363.4.6

Maher, J. P. (2017). *Investigating the functional and evolutionary significance of Group B Sox genes in arthropods* (Ph.D. thesis), University of Cambridge.

Martin, P., Dorn, N. J., Kawai, T., van der Heiden, C., & Scholtz, G. (2010). The enigmatic Marmorkrebs (marbled crayfish) is the parthenogenetic form of *Procambarus fallax* (Hagen, 1870). *Contributions to Zoology*, *79*, 107–118. https://doi.org/10.1163/18759866-07903003

Martin, P., Kohlmann, K., & Scholtz, G. (2007). The parthenogenetic Marmorkrebs (marbled crayfish) produces genetically uniform offspring. *Die Naturwissenschaften*, *94*, 843–846. https://doi.org/10.1007/s00114-007-0260-0

Martin, P., Thonagel, S., & Scholtz, G. (2016). The parthenogenetic Marmorkrebs (Malacostraca: Decapoda: Cambaridae) is a triploid organism. *Journal of Zoological Systematics and Evolutionary Research*, *54*, 13–21. https://doi.org/10.1111/jzs.12114

McKimmie, C., Woerfel, G., & Russell, S. (2005). Conserved genomic organisation of Group B Sox genes in insects. *BMC Genetics*, *6*, 26. https://doi.org/10.1186/1471-2156-6-26

McMurrich, J. (1895). Embryology of the isopod Crustacea. *Journal of Morphology*, *11*, 63-154. https://doi.org/10.1002/jmor.1050110103

Miller, M. A., Pfeiffer, W., & Schwartz, T. (2010). *Creating the CIPRES Science Gateway for inference of large phylogenetic trees*. Proceedings of the Gateway Computing Environments Workshop (GCE), 14 Nov. 2010 (pp. 1–8).

Negre, B., & Simpson, P. (2009). Evolution of the *achaete-scute* complex in insects: Convergent duplication of proneural genes. *Trends in Genetics*, *25*, 147–152. https://doi.org/10.1016/j.tig.2009.02.001

Nieto, M. A. (2002). The *snail* superfamily of zinc-finger transcription factors. *Nature Review Molecular Cell Biology*, *3*, 155–166. https://doi.org/10.1038/nrm757

Overton, P. M., Meadows, L. A., Urban, J., & Russell, S. (2002). Evidence for differential and redundant function of the Sox genes *Dichaete* and *SoxN* during CNS development in *Drosophila*. *Development*, *129*, 4219–4228. https://doi.org/10.1242/dev.129.18.4219

Paese, C. L. B., Leite, D. J., Schönauer, A., McGregor, A. P., & Russell, S. (2018). Duplication and expression of Sox genes in spiders. *BMC Evolutionary Biology*, *18*, 205. https://doi.org/10.1186/s12862-018-1337-4

Paese, C. L. B., Schoenauer, A., Leite, D. J., Russell, S., & McGregor, A. P. (2018). A SoxB gene acts as an anterior gap gene and regulates posterior segment addition in a spider. *eLife*, *7*, e37567. https://doi.org/10.7554/eLife.37567

Pioro, H. L., & Stollewerk, A. (2006). The expression pattern of genes involved in early neurogenesis suggests distinct and conserved functions in the diplopod *Glomeris marginata*. *Development, Genes and Evolution*, *216*, 417–430. https://doi.org/10.1007/s00427-006-0078-3

Reichardt, I., Bonnay, F., Steinmann, V., Loedige, I., Burkard, T. R., Meister, G., & Knoblich, J. A. (2018). The tumor suppressor Brat controls neuronal stem cell lineages by inhibiting Deadpan and Zelda. *EMBO Reports*, *19*, 102–117. https://doi.org/10.15252/embr.201744188

Reichenbach, H. (1886). Studien zur Entwicklungsgeschichte des Flusskrebses. *Abhandlungen der Senckenbergischen Naturforschenden Gesellschaft*, *14*, 1–137.

Robinow, S., Campos, A. R., Yao, K. - M., & White, K. (1988). The *elav* gene product of *Drosophila*, required in neurons, has three RNP consensus motifs. *Science*, *242*, 1570–1572. https://doi.org/10.1126/science.3144044

Robinow, S., & White, K. (1988). The locus *elav* of *Drosophila melanogaster* is expressed in neurons at all developmental stages. *Developmental Biology*, *126*, 294–303. https://doi.org/10.1016/0012-1606(88)90139-X

Robinow, S., & White, K. (1991). Characterization and spatial distribution of the ELAV protein during *Drosophila melanogaster* development. *Journal of Neurobiology*, *22*, 443–461. https://doi.org/10.1002/neu.480220503

Ronquist, F., Teslenko, M., van der Mark, P., Ayres, D., Darling, A., Höhna, S., Larget, B., Liu, L., Suchard, M. A., & Huelsenbeck, J. (2012). Efficient Bayesian phylogenetic inference and model selection across a large model space. *Systematic Biology*, *61*, 539–542. https://doi.org/10.1093/sysbio/sys029

Russell, S. R. H., Sánchez-Soriano, N., Wright, C. R., & Ashburner, M. (1996). The *Dichaete* gene of *Drosophila melanogaster* encodes a SOX-domain protein required for embryonic segmentation. *Development*, *122*, 3669–3676. https://doi.org/10.1242/dev.122.11.3669

Sánchez-Soriano, N., & Russell, S. (2000). Regulatory mutations of the *Drosophila* Sox gene *Dichaete* reveal new functions in embryonic brain and hindgut development. *Development*, *220*, 307–321.

Sandeman, D. C., Bazin, F., & Beltz, B. S. (2011). Adult neurogenesis: Examples from the decapod crustaceans and comparisons with mammals. *Arthropod Structure and Development*, *40*, 258–275. https://doi.org/10.1016/j.asd.2011.03.001

Sandeman, R., & Sandeman, D. (1991). Stages in the development of the embryo of the fresh-water crayfish *Cherax destructor*. *Roux's Archives of Developmental Biology*, *200*, 27–37. https://doi.org/10.1007/BF02457638

Schmidt, M. (1997). Continuous neurogenesis in the olfactory brain of adult shore crabs, *Carcinus maenas*. *Brain Research*, *762*, 131–143. https://doi.org/10.1016/S0006-8993(97)00376-4

Schmidt, M. (2001). Neuronal differentiation and long-term survival of newly generated cells in the olfactory midbrain of the adult spiny lobster, *Panulirus argus*. *Journal of Neurobiology*, *48*, 181–203. https://doi.org/10.1002/neu.1050

Schmidt, M. (2007). Identification of putative neuroblasts at the base of adult neurogenesis in the olfactory midbrain of the spiny lobster, *Panulirus argus*. *The Journal of Comparative Neurology*, *503*, 64–84. https://doi.org/10.1002/cne.21366

Schmidt, M., & Derby, C. D. (2011). Cytoarchitecture and ultrastructure of neural stem cell niches and neurogenic complexes maintaining adult neurogenesis in the olfactory midbrain of spiny lobsters, *Panulirus argus*. *The Journal of Comparative Neurology*, *519*, 2283–2319. https://doi.org/10.1002/cne.22657

Schmidt, M., & Harzsch, S. (1999). Comparative analysis of neurogenesis in the central olfactory pathway of adult decapod crustaceans by *in vivo* BrdU labeling. *Biological Bulletin*, *196*, 127–136. https://doi.org/10.2307/1542558

Scholtz, G. (1990). The formation, differentiation and segmentation of the post-naupliar germ band of the amphipod *Gammarus pulex* L. (Crustacea, Malacostraca, Peracarida). *Proceedings of the Royal Society of London B*, *239*, 163–211.

Scholtz, G. (1992). Cell lineage studies in the crayfish *Cherax destructor* (Crustacea, Decapoda): Germ band formation, segmentation, and early neurogenesis. *Roux's Archives of Developmental Biology*, *202*, 36–48. https://doi.org/10.1007/BF00364595

Scholtz, G. (1993). Teloblasts in decapod embryos: An embryonic character reveals the monophyletic origin of freshwater crayfishes (Crustacea, Decapoda). *Zoologischer Anzeiger*, *230*, 45–54.

Scholtz, G., Braband, A., Tolley, L., Reimann, A., Mittmann, B., Lukhaup, C., Steuerwald, F., & Vogt, G. (2003). Parthenogenesis in an outsider crayfish. *Nature*, *421*, 806. https://doi.org/10.1038/421806a

Scholtz, G., & Wolff, C. (2013). Arthropod embryology: Cleavage and germ band development. In A. Minelli, G. Boxshall & G. Fusco (Eds.), *Arthropod biology and evolution. molecules, development, morphology* (pp. 63–89). Springer Verlag.

Schwentner, M., Combosch, D., Nelson, J., & Giribet, G. (2017). A phylogenomic solution to the origin of insects by resolving crustacean-hexapod relationships. *Current Biology*, *27*, 1818–1824.e5. https://doi.org/10.1016/j.cub.2017.05.040

Schwentner, M., Richter, S., Rogers, D. C., & Giribet, G. (2018). Tetraconatan phylogeny with special focus on Malacostraca and Branchiopoda: Highlighting the strength of taxon-specific matrices in phylogenomics. *Proceedings of the Royal Society B*, *285*, 20181524. https://doi.org/10.1098/rspb.2018.1524

Seitz, R., Vilpoux, K., Hopp, U., Harzsch, S., & Maier, G. (2005). Ontogeny of the Marmorkrebs (marbled crayfish): A parthenogenetic crayfish with unknown origin and phylogenetic position. *Journal of Experimental Zoology*, *303A*, 393–405. https://doi.org/10.1002/jez.a.143

Shiino, S. M. (1942). Studies on the embryology of *Squilla oratoria* de Haan. *Memoirs of the College of Science, Kyoto Imperial University, Series B*, *17*, 77–174.

Shiino, S. M. (1950). Studies on the embryonic development of *Panulirus japonicus* (von Siebold). *Journal of the Faculty of Fisheries, Prefectural University of Mie*, *1*, 1–168.

Sintoni, S., Benton, J. L., Beltz, B. S., Hansson, B. S., & Harzsch, S. (2012). Neurogenesis in the central olfactory pathway of adult decapod crustaceans: Development of the neurogenic niche in the brains of procambarid crayfish. *Neural Development*, *7*, 1. https://doi.org/10.1186/1749-8104-7-1

Skeath, J. B., & Carroll, S. B. (1992). Regulation of proneural gene expression and cell fate during neuroblast segregation in the *Drosophila* embryo. *Development*, *114*, 939–946. https://doi.org/10.1242/dev.114.4.939

Skeath, J. B., & Thor, S. (2003). Genetic control of *Drosophila* nerve cord development. *Current Opinion in Neurobiology*, *13*, 8–15. https://doi.org/10.1016/S0959-4388(03)00007-2

Soller, M., & White, K. (2003). ELAV inhibits 3'-end processing to promote neural splicing of ewg pre-mRNA. *Genes and Development*, *17*, 2526–2538. https://doi.org/10.1101/gad.1106703

Sonoda, J., & Wharton, R. P. (2001). *Drosophila* Brain Tumor is a translational repressor. *Genes and Development*, *15*, 762–773. https://doi.org/10.1101/gad.870801

Southall, T. D., & Brand, A. H. (2009). Neural stem cell transcriptional networks highlight genes essential for nervous system development. *The EMBO Journal*, *28*, 3799–3807. https://doi.org/10.1038/emboj.2009.309

Spana, E. P., & Doe, C. Q. (1995). The prospero transcription factor is asymmetrically localized to the cell cortex during neuroblast mitosis in *Drosophila*. *Development*, *121*, 3187–3195. https://doi.org/10.1242/dev.121.10.3187

Stollewerk, A. (2016). A flexible genetic toolkit for arthropod neurogenesis. *Philosophical Transactions of the Royal Society of London*, *371*, 20150044. https://doi.org/10.1098/rstb.2015.0044

Stollewerk, A., Tautz, D., & Weller, M. (2003). Neurogenesis in the spider: New insights from comparative analysis of morphological processes and gene expression patterns. *Arthropod Structure and Development*, *32*, 5–16. https://doi.org/10.1016/S1467-8039(03)00041-0

Stollewerk, A., Weller, M., & Tautz, D. (2001). Neurogenesis in the spider *Cupiennius salei*. *Development*, *128*, 2673–2688. https://doi.org/10.1242/dev.128.14.2673

Sullivan, J. M., & Beltz, B. S. (2005). Newborn cells in the adult crayfish brain differentiate into distinct neuronal types. *Journal of Neurobiology*, *65*, 157–170. https://doi.org/10.1002/neu.20195

Sullivan, J. M., Benton, J. L., Sandeman, D. C., & Beltz, B. S. (2007). Adult neurogenesis: A common strategy across diverse species. *The Journal of Comparative Neurology*, *500*, 574–584. https://doi.org/10.1002/cne.21187

Sullivan, J. M., Sandeman, D. C., Benton, J. L., & Beltz, B. S. (2007). Adult neurogenesis and cell cycle regulation in the crustacean olfactory pathway: From glial precursor to differentiated neurons. *Journal of Molecular Histology*, *38*, 527–542. https://doi.org/10.1007/s10735-007-9112-7

Thomas, J. B., Bastiani, M. J., Bate, C. M., & Goodman, C. S. (1984). From grasshopper to *Drosophila*: A common plan for neuronal development. *Nature*, *310*, 203–207. https://doi.org/10.1038/310203a0

Ungerer, P., Eriksson, B. J., & Stollewerk, A. (2011). Neurogenesis in the water flea *Daphnia magna* (Crustacea, Branchiopoda) suggests different mechanisms of neuroblast formation in insects and crustaceans. *Developmental Biology*, *357*, 42–52. https://doi.org/10.1016/j.ydbio.2011.05.662

Ungerer, P., Eriksson, B. J., & Stollewerk, A. (2012). Unravelling the evolution of neural stem cells in arthropods: Notch signalling in neural stem cell development in the crustacean *Daphnia magna*. *Developmental Biology*, *371*, 302–311. https://doi.org/10.1016/j.ydbio.2012.08.025

Ungerer, P., Geppert, M., & Wolff, C. (2011). Axogenesis in the central and peripheral nervous system of the amphipod crustacean *Orchestia cavimana*. *Integrative Zoology*, *6*, 28–44. https://doi.org/10.1111/j.1749-4877.2010.00227.x

Ungerer, P., & Scholtz, G. (2008). Filling the gap between identified neuroblasts and neurons in crustaceans adds new support for Tetraconata. *Proceedings of the Royal Society B*, *275*, 369–376. https://doi.org/10.1098/rspb.2007.1391

Urbach, R., Schnabel, R., & Technau, G. M. (2003). The pattern of neuroblast formation, mitotic domains and proneural gene expression during early brain development in *Drosophila*. *Development*, *130*, 3589–3606. https://doi.org/10.1242/dev.00528

Urbach, R., & Technau, G. M. (2003). Early steps in building the insect brain: Neuroblast formation and segmental patterning in the developing brain of different insect species. *Arthropod Structure and Development*, *32*, 103–123. https://doi.org/10.1016/S1467-8039(03)00042-2

Vaessin, H., Grell, E., Wolff, E., Bier, E., Jan, L. Y., & Jan, Y. N. (1991). *prospero* is expressed in neuronal precursors and encodes a nuclear protein that is involved in the control of axonal outgrowth in *Drosophila*. *Cell*, *67*, 941–953. https://doi.org/10.1016/0092-8674(91)90367-8

Vilpoux, K., Sandeman, R. E., & Harzsch, S. (2006). Early embryonic development of the central nervous system in the Australian crayfish and the Marbled crayfish (Marmorkrebs). *Development, Genes and Evolution*, *216*, 209–223. https://doi.org/10.1007/s00427-005-0055-2

Vogt, G., Falckenhayn, C., Schrimpf, A., Schmid, K., Hanna, K., Panteleit, J., Helm, M., Schulz, R., & Lyko, F. (2015). The marbled crayfish as a paradigm for saltational speciation by autopolyploidy and parthenogenesis in animals. *Biology Open*, *4*, 1583–1594. https://doi.org/10.1242/bio.014241

Wei, J., Glaves, R. S., Sellars, M. J., Xiang, J., & Hertzler, P. L. (2016). Expression of the prospective mesoderm genes *twist*, *snail*, and *mef2* in penaeid shrimp. *Development Genes and Evolution*, *226*, 317–324. https://doi.org/10.1007/s00427-016-0544-5

Wei, L., Lee, S., Majumdar, S., Zhang, B., Sanfilippo, P., Joseph, B., Miura, P., Soller, M., & Lai, E. C. (2020). Overlapping activities of ELAV/Hu family RNA binding proteins specify the extended neuronal 3' UTR landscape in *Drosophila*. *Molecular Cell*, *80*, 140–155.e6. https://doi.org/10.1016/j.molcel.2020.09.007

Weygoldt, P. (1961). Beitrag zur Kenntnis der Ontogenie der Dekapoden: Embryologische Untersuchungen an *Palaemonetes varians* (Leach). *Zoologische Jahrbücher der Anatomie*, *79*, 223–270.

Wheeler, S. R., Carrico, M. L., Wilson, B. A., Brown, S. J., & Skeath, J. B. (2003). The expression and function of the *achaete-scute* genes in *Tribolium castaneum* reveals conservation and variation in neural pattern formation and cell fate specification. *Development*, *130*, 4373–4381. https://doi.org/10.1242/dev.00646

Wheeler, S. R., & Skeath, J. B. (2005). The identification and expression of *achaete-scute* genes in the branchiopod crustacean *Triops longicaudatus*. *Gene Expression Patterns*, *5*, 695–700. https://doi.org/10.1016/j.modgep.2005.02.005

Whitington, P. M., Harris, K. L., & Leach, D. (1996). Early axonogenesis in the embryo of a primitive insect, the silverfish *Ctenolepisma longicaudata*. *Roux's Archives of Developmental Biology*, *205*, 272–281. https://doi.org/10.1007/BF00365805

Whitington, P. M., Leach, D., & Sandeman, R. (1993). Evolutionary change in neural development within the arthropods: Axonogenesis in the embryos of two crustaceans. *Development*, *118*, 449–461. https://doi.org/10.1242/dev.118.2.449

Wittfoth, C., & Harzsch, S. (2018). Adult neurogenesis in the central olfactory pathway of dendrobranchiate and caridean shrimps: New insights into the evolution of the deutocerebral proliferative system in reptant decapods. *Developmental Neurobiology*, *78*, 757–774. https://doi.org/10.1002/dneu.22596

Younossi-Hartenstein, A., Nassif, C., Green, P., & Hartenstein, V. (1996). Early neurogenesis in the *Drosophila* brain. *The Journal of Comparative Neurology*, *370*, 313–329. https://doi.org/10.1002/(SICI)1096-9861(19960701)370:3%3c313::AID-CNE3%3e3.0.CO;2-7

Zehnder, H. (1934). Über die Embryonalentwicklung des Flusskrebses. Teil 2: Die Ausbildung der äußeren Körperform von *Astacus fluviatilis* (Rond.) L. und *Astacus torrentium* (Schrank) von der Gastrulation bis zum entwickelten Tier. *Acta Zoologica*, *15*, 85–148.

Zhao, G., Boekhoff-Falk, G., Wilson, B. A., & Skeath, J. B. (2007). Linking pattern formation to cell-type specification: Dichaete and Ind directly repress *achaete* gene expression in the *Drosophila* CNS. *Proceedings of the National Academy of Sciences*, *104*, 3847–3852. https://doi.org/10.1073/pnas.0611700104

Zhao, G., & Skeath, J. B. (2002). The Sox-domain containing gene *Dichaete/fish-hook* acts in concert with *vnd* and *ind* to regulate cell fate in the *Drosophila* neuroectoderm. *Development*, *129*, 1165–1174. https://doi.org/10.1242/dev.129.5.1165

Zhong, L., Wang, D., Gan, X., Yang, T., & He, S. (2011). Parallel expansions of *Sox* transcription factor group B predating the diversifications of the arthropods and jawed vertebrates. *PLoS ONE*, *6*, e16570. https://doi.org/10.1371/journal.pone.0016570

SUPPORTING INFORMATION

Additional supporting information may be found in the online version of the article at the publisher's website.

How to cite this article: Brenneis, G., Schwentner, M., Giribet, G., & Beltz, B. S. (2021). Insights into the genetic regulatory network underlying neurogenesis in the parthenogenetic marbled crayfish *Procambarus virginalis*. *Developmental Neurobiology*, *81,* 939–974. https://doi.org/10.1002/dneu.22852